AB INITIO STUDIES OF PENTACENE ON AG(111) SURFACES

A THESIS SUBMITTED TO
THE GRADUATE SCHOOL OF NATURAL AND APPLIED SCIENCES
OF
MIDDLE EAST TECHNICAL UNIVERSITY

BY

İLKER DEMİROĞLU

IN PARTIAL FULFILLMENT OF THE REQUIREMENTS
FOR
THE DEGREE OF MASTER OF SCIENCE
IN
CHEMISTRY

JANUARY 2010

Approval of the thesis:

AB INITIO STUDIES OF PENTACENE ON AG(111) SURFACES

submitted by **İLKER DEMİROĞLU** in partial fulfillment of the requirements for the degree of **Master of Science in Chemistry Department, Middle East Technical University** by,

Prof. Dr. Canan Özgen
Dean, Graduate School of **Natural and Applied Sciences** _____

Prof. Dr. Ahmet Önal
Head of Department, **Chemistry** _____

Assist. Prof. Dr. Mehmet Fatih Danışman
Supervisor, **Chemistry Department, METU** _____

Prof. Dr. Şinasi Ellialtıoğlu
Co-supervisor, **Physics Department, METU** _____

Examining Committee Members:

Assoc. Prof. Dr. Ersen Mete
Physics Department, Balikesir University _____

Assist. Prof. Dr. Mehmet Fatih Danışman
Chemistry Department, METU _____

Prof. Dr. Şinasi Ellialtıoğlu
Physics Department, METU _____

Assist. Prof. Dr. Daniele Toffoli
Chemistry Department, METU _____

Assist. Prof. Dr. Okan Esentürk
Chemistry Department, METU _____

Date: _____

I hereby declare that all information in this document has been obtained and presented in accordance with academic rules and ethical conduct. I also declare that, as required by these rules and conduct, I have fully cited and referenced all material and results that are not original to this work.

Name, Last Name: İLKER DEMİROĞLU

Signature :

ABSTRACT

AB INITIO STUDIES OF PENTACENE ON AG(111) SURFACES

Demiroğlu, İlker

M.S., Department of Chemistry

Supervisor : Assist. Prof. Dr. Mehmet Fatih Danışman

Co-Supervisor : Prof. Dr. Şinasi Ellialtıoğlu

January 2010, 59 pages

In this work pentacene adsorption on both flat and stepped Ag(111) surfaces were investigated by using Density Functional Theory within Projected Augmented Wave method. On the flat Ag(111) surface favorable adsorption site for a single pentacene molecule was determined to be the bridge site with an angle of 60° between pentacene molecular long axis and $[0\bar{1}1]$ lattice direction. Potential energy surface was found to be flat, especially along lattice directions. Diffusion and rotation barriers for pentacene on this surface were found to be smaller than 40 meV indicating the possibility of a two dimensional gas phase. Calculated adsorption energies for the flat surface indicate a weak interaction between molecule and the surface indicating physisorption. On the flat surface monolayer case is found to have lower adsorption energy than the isolated case due to pentacene−pentacene interactions. On the stepped Ag(233) surface, close to the step edge, adsorption energy increased significantly due to the stronger interaction between pentacene molecule and low coordinated silver step atoms. On the terraces of this surface, far from step edges, however a flat potential energy surface was observed similar to the case of flat Ag(111) surface. On the stepped surface pentacene found its favorable configuration as parallel to the step with a tilt angle similar to the observed thin film phase of pentacene on Ag(111) surface. Pentacene molecule showed small distortions on

stepped surface and are closer to the silver step atoms 1 Å more than the case of flat surface, hinting a chemical interaction as well as van der Waals interactions. However on Ag(799) surface, the perpendicular orientation of the pentacene molecule to the step direction showed no strong interaction due to less matching of carbon atoms with silver step atoms.

Keywords: Pentacene, Adsorption on Silver (111) surface, Density Functional Theory (DFT)

ÖZ

AB INITIO YÖNTEMLERLE AG(111) YÜZEYLERİNDE PENTACENE TUTUNMASI

Demiroğlu, İlker
Yuksek Lisans, Kimya Bölümü
Tez Yöneticisi : Assist. Prof. Dr. Mehmet Fatih Danışman
Ortak Tez Yöneticisi : Prof. Dr. Şinasi Ellialtıoğlu

Ocak 2010, 59 sayfa

Bu çalışmada pentacene molekülünün düz ve basamaklı Ag(111) yüzeylerinde tutunmasının Yoğunluk Fonksiyoneli Teorisi kulanılarak incelendi. Düz Ag(111) yüzeyinde pentacene molekülü için tercih edilen tutunma bölgesi pentacene'in uzun molekküler ekseniyle $[0\bar{1}1]$ yapı yönü arasında 60 derecelik açı yapacak şekilde köprü pozisyonu olduğu tespit edildi. Potansiyel enerji yüzeyinin özellikle yapı yönleri doğrultusunda düz olduğu gözlemlendi. Yüzey üzerinde difüzyon ve dönme bariyerlerinin 40 meV tan daha küçük olduğu gözlemlenerek iki boyutlu gaz fazının yüzey üzerinde mümkün olduğu görüldü. Düz yüzey için hesaplanan tutunma enerjileri molekülle yüzey arasında zayıf van der Waals etkilesimlerinin olduğunu ve fiziksel bir tutunma gerçekleştiğini gösterdi. Düz yüzey üzerinde kaplanma oranı artırıldıkça, başka bir deyişle yüzeyde izole bir molekülden bir katman tutunmaya geçildiğinde moleküller arası etkileşimler dolayısıyla tutunma enerjisinin azaldığı gözlendi. Basamaklı yüzeyde tutunma enerjisinin pentacene basamağa yaklaştıkça arttığı gözlemlendi. Basamaklı yüzeyde, difüzyon enerji bariyerlerinin molekülle az koordine olmuş gümüş basamak atomları arasındaki güçlü etkileşimler sebebiyle büyük ölçüde arttığı gozlemlendi. Fakat pentacene molekülünün basamaktan uzakta kaldığı zaman teras üzerinde potansiyel enerji yüzeyinin düz yüzeydeki gibi düz olduğu gözlendi. Basamaklı yüzey üzerinde pentacene molekülü

çok tabakalı katmanlardakine denk gelen bir açıyla basamağa paralel olarak yüzey üzerinde en uygun tutunma pozisyonunu buldu. Basamaklı yüzeydeki tutunma sırasında pentacene molekülü üzerinde ufak yapısal değişimler gözlemlendi. Pentacene mole-külü basamaktaki gümüş atomlarına düz yüzeydekine göre 1 Å daha yakınlaşarak van der Waals etlileşmelerinin yanısıra kimyasal bağ ipuçları gösterdi. Basamaklı Ag(799) yüzeyinde ise basamağa dik olarak yerleştirilen pentacene molekülü, daha az karbon atomunun basamaktaki gümüş atom-larıyla denk gelmesi sebebiyle Ag(233) yüzeyindeki paralel konfigürasyon gibi güçlü etk-ilesme göstermedi.

Anahtar Kelimeler: Pentacene, Gümüş (111) Yüzeyinde Tutunma, Yoğunluk Fonksiyoneli Teorisi (DFT)

To my family

ACKNOWLEDGMENTS

I express my appreciation to my suprvisors Assist. Prof. Dr. Fatih Danışman and Prof. Dr. Şinasi Ellialtıoğlu for their guidance, insight and support througout this study.

I would like to thank to Assoc. Prof. Dr. Ersen Mete for his help during my research.

I would like to thank to my friends Aysun, Ebru, Hava and Şuheda for their support and encouregement as well as for their friendship.

I would like to thank to Atılım University Chemistry Group for their support during my graduate education period.

TABLE OF CONTENTS

LIST OF TABLES

TABLES

LIST OF FIGURES

FIGURES

CHAPTER 1

INTRODUCTION

1.1 Organic Semiconductors

Semiconductors are a group of materials having conductivities between those of metals and insulators. Devices made from semiconductor materials are the foundation of modern electronics, including radio, computers, telephones, and many other devices. Organic semiconductors attract great interest because of their potential advantages over Si-based electronics, particularly in large area, low cost and flexible applications. Semiconductors based on organic molecular components are mainly composed of hydrogen, carbon and oxygen. Unlike inorganic semiconductors that are crystalline with band-like charge transport, organic semiconductors are amorphous or polycrystalline in which the charge transport occurs through hopping of charges between delocalized π molecular orbitals. The semiconducting or conducting properties of organic moelcules can be attributed to the special chemical characteristic of carbon: carbon atoms can form double bonds between each other, as shown in Figure 1.1. One of these bonds, called as a σ bond , and the second, known as a π bond. The σ electrons mostly remain between the carbon nuclei, while the π electrons are delocalized over the neighboring nuclei in a conjugated system, by which the electrons can gain some freedom to move along the conjugation length. The formation of delocalized π molecular orbitals defines the frontier electronic levels: the highest occupied molecular orbital (HOMO) and the lowest unoccupied molecular orbital (LUMO). The HOMO and LUMO levels determine the electrical and optical properties of the organic semiconductor molecules.

Organic semiconductors can be categorized into two groups, small-molecule organic semiconductors and polymer organic semiconductors. In small-molecule organic semiconductors,

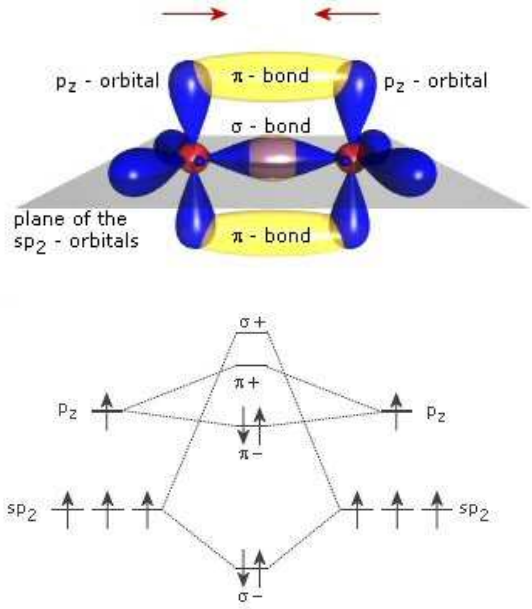

Figure 1.1: Scheme of the orbitals and bonds for two sp^2 hybridized carbon atoms [3].

the carbon atoms form larger molecules typically with benzene rings as the basic unit and π electrons become delocalized through the molecules. In polymer organic semiconductors the carbon atoms form a long chain and π electrons become delocalized along the chain and form a one-dimensional π-conjugated system.The development of organic semiconductors was pioneered in the 1950s by Martin Pope and colleagues, who performed studies of the ground- and excited-state electronic structure of model molecules and crystals, such as anthracene. [1] Also organic electronics has its root in the discovery of the conducting properties of doped polyacetylene in 1977 [2], which gained the Nobel Prize in Chemistry in 2000. This remarkable studies opened up the field of organic electronics, and new applications for semiconducting organic materials. Organic electronics are based on organic semiconductors and mainly used in three main technological areas, which are organic light-emitting diodes (OLEDs), organic photovolatic solar cells and organic electronic circuits based on organic thin-film field-effect transistors (OFETs). OFETs have recently gained attention as building blocks for electronic applications like radio-frequency identification tags (RFID) [4], drivers for electronic papers [5] and driving circuits for flat panel displays (FPDs) [6].

1.2 Organic Thin Film Transistors

Field-effect transistors (FETs) are the fundamental devices for microelectronics, which are commonly used to amplify or switch electronic signals. OFETs are transistors that uses organic semiconductors as active layer. With the remarkable progress in the processing of organic semiconductors into devices, the mobility of the OFETs has surpassed that of amorphous-Si TFTs [7, 8]. The OFETs are categorized into two with respect to the type of the charge carriers, n-type and p-type, where in n-type the majority of carriers are electrons whereas in the p-type holes. A typical OFET is composed of a gate electrode, a gate dielectric layer, an organic semiconductor layer and source-drain electrodes [9]. There are four common types of OFETs as shown in Figure 1.2. When a gate voltage is applied the carriers accumulate on the semiconductor layer interface and form a conductive channel. Then carriers move from the source electrode into the semiconductor layer and travel through the channel to the drain electrode. In OFETs, the most important processes are the charge injection in the electrode/semiconductor interface and charge transport along the interface between dielectric and semiconductor layers [10, 11]. Therefore, the properties of these interfaces influence the device characteristics drastically.

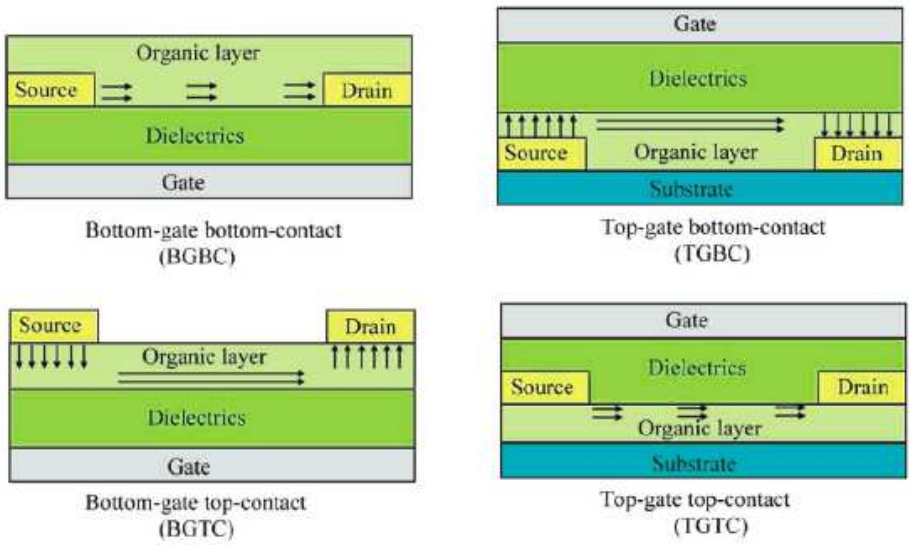

Figure 1.2: Carrier injection and transport scheme of four typical OFET geometries [9].

1.3 Pentacene

Pentacene was exposed to extensive research in recent years due to its use in organic electronics. Pentacene ($C_{22}H_{14}$) is one of the acene molecules, which is made up of five fused benzene rings (Figure 1.3). Pentacene is easily synthesized via quinone [12] and commercially available.

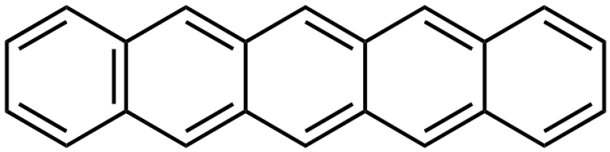

Figure 1.3: Structure of pentacene.

Acenes are an extended class of fused polycyclic hydrocarbons. Applications of these materials is very wide from the use as moth repellents to the starting materials for artificial dyes. More recently, these molecules have received attention due to their electronic properties, low-lying HOMO energy levels and strong two-dimensional electronic interactions in the solid state.In acene molecules the carbon atoms are bonded to three other atoms, which leaves one electron free in a delocalized p_z-orbital. π orbitals of neighboring atoms overlap to form π bonds, which extend along the molecule. This π system is responsible for an important part of the intramolecular conduction. Pentacene is the most commonly used organic semiconductor [13, 14, 15] in thin-film transistors among all acenes, where it serves as the benchmark [16]. The first pentacene transistors, reported by Horowitz et al. in the early 1990s, had a mobility of 0.002 cm^2/Vs in a top-contact device [17, 18]. Purification of pentacene by sublimation improved the mobility to 0.038 cm^2/Vs for a bottom-contact device [19, 20]. With high-purity materials, further optimization of film morphology by employing self-assembled monolayers on the dielectric surface led to dramatic increases in device mobility: greater than 1 cm^2/Vs in a bottom-contact device [21]. Nowadays fabricating pentacene TFT's with hole mobilities of more than 1 cm^2/Vs have become an almost routine process [7] (Figure 1.4).

Pentacene forms bulk crystals with herringbone structure in which the face of one molecule is close to the edge of another. Figure 1.5 shows the structure of a layer within a bulk pentacene

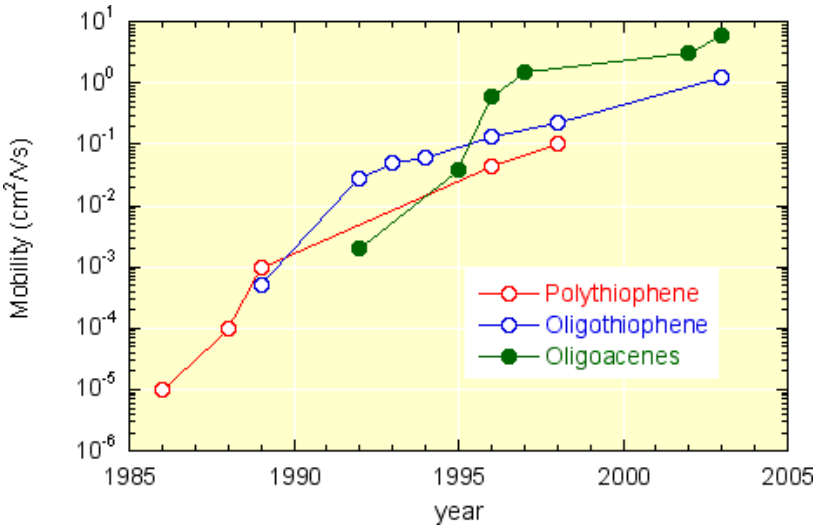

Figure 1.4: Observed mobilities via common organic semicondutors in recent years [13].

crystal. The bulk solid consists of a stack of these layers. Pentacene has a triclinic crystal structure with a=7.90 Å, b=6.06 Å and c=16.01 Å. The unit cell contains two nonequivalent molecules and the longitudinal axes of them have different orientations with respect to the surface normal. The longitudinal axes of two molecules are tilted by 22.1° and 20.3° with respect to the surface normal [22]. At least four different polymorphic structures of pentacene with different intermolecular spacings have been reported [23].

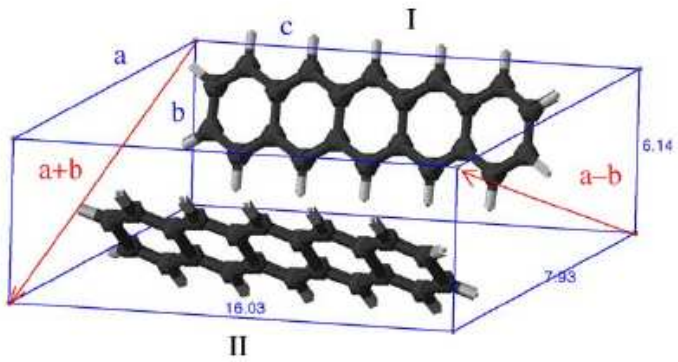

Figure 1.5: Bulk structure of pentacene [24].

1.4 Thin Film Morphology

It is widely recognized that transport properties of crystalline organic films are strongly dependent on the intermolecular overlap within the semiconductor layer [25, 26, 27]. Also the bandwidths of the valance and conduction bands which determine the charge migration mechanism are found to depend strongly on the crystallographic directions [24]. In their study, Endres et al. reported theoretical band structure (Figure 1.6) calculations on bulk pentacene within density functional theory with localized pseudo-atomic orbitals. They have found that bandwiths along the triclinic lattice vectors are much smaller than that of stacking directions.

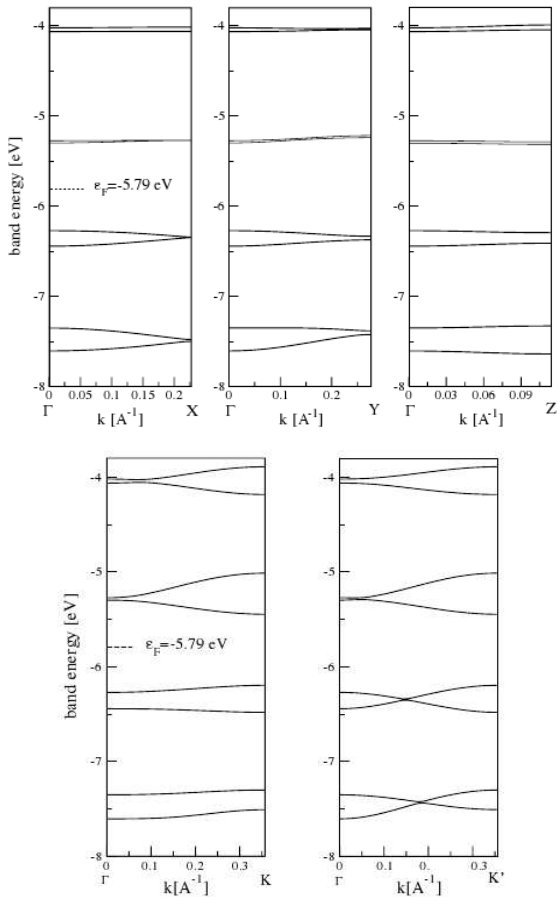

Figure 1.6: Band structures of bulk pentacene along lattice and stacking directions [25].

In another study Parisse et al. [25] compared the band-structures of thin film and bulk phases by using DFT calculations. They have reported 0.2 eV smaller band gap (Figure 1.7) for thin

film phase with larger bandwiths for HOMO and LUMO states than in the bulk structure. Since the mobility is related with the thin film morphology, initial studies were focused on the thin film structures of organic semiconductors, particularly on pentacene, which has relatively high hole mobility [7] and high on-off current ratios in OFETs [28].

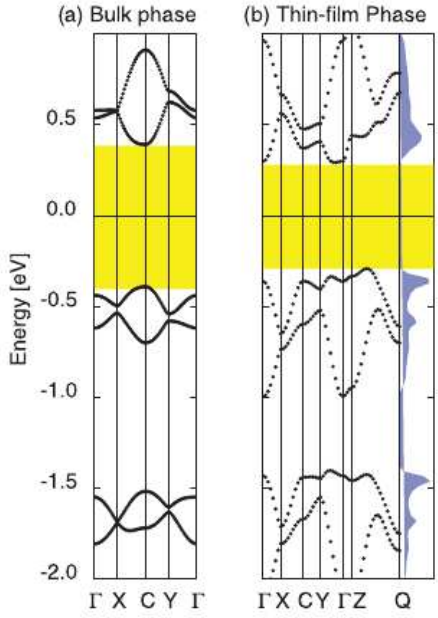

Figure 1.7: Band structures of (a) bulk and (b) thin-film phases of pentacene [25].

1.4.1 SiO_2 Surface

Since most TFTs uses SiO_2 as the dielectric layer, structural [16, 29, 30, 23] and electronic [31, 32, 33, 34] properties of pentacene thin films on this substrate is heavily investigated. In these studies it is found that pentacene molecules prefer standing up on the substrate with their long molecular axis perpendicular to the surface with different thin film morphologies, which are bulk like herringbone structures slightly changing with the growth parameters [35]. In an experimental study, Dimitrakopoulos et al. [16] found that morphology of the thin film drastically affect the mobility. They have reported mobility values for amorphous, thin film and a mixture of thin film and bulk phases grown at different substrate temperatures (Figure 1.8). They have observed maximum mobility for the ordered thin film phase and low mobility for disordered growth.

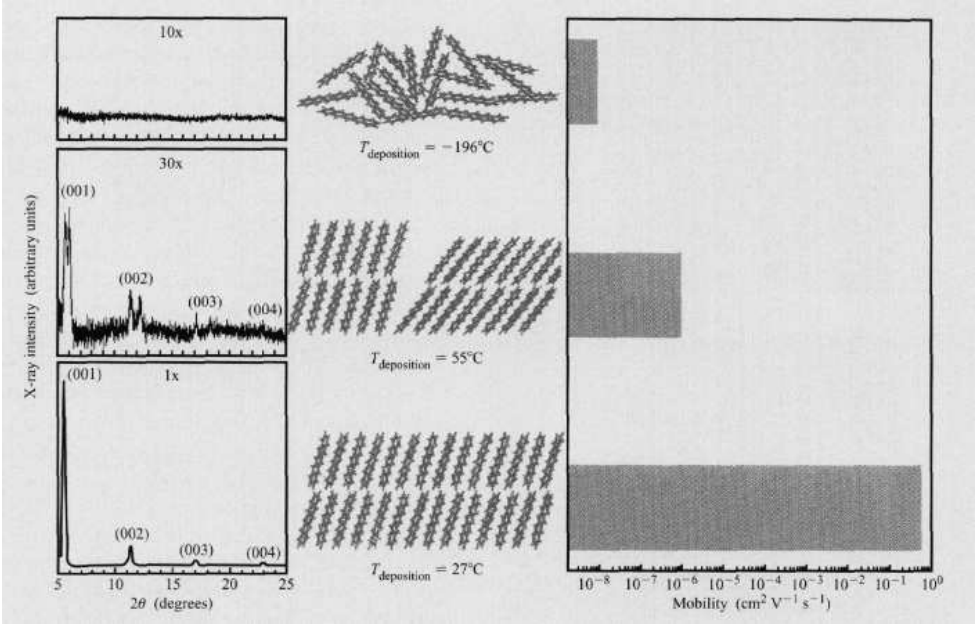

Figure 1.8: mobility values for amorphous, thin film and a mixture of thin film and bulk phases of pentacene [19].

Since the mobility depends on the morphology of the pentacene thin film, studies continued with the optimization of the growth parameters for achieving thin films leading to best device performance [36, 37, 38]. Pentacene thin films are generally prepared by molecular beam deposition under high vacuum. [30]. Deposition starts with the evaporation of organic molecules. Then these molecules are sent on the substrate material with a controlled flux. Incoming molecules adsorb on the surface and start to diffuse on the surface, which can desorp or create islands by finding other adsorbed molecules on the surface (Figure 1.9). Diffusion is mainly controlled by the substrate temperature. Incoming molecules can be sent also with an initial extra kinetic energy to control difussion without changing substrate temperature with supersonic molecular beam method [52].

The main factors affecting film growth are, nature of the substrate, substrate temperature, deposition rate and the kinetic energy of molecular beam. In general three classes of growth modes are seen in molecular beam deposition [38] which are Frank-van der Merwe, Stranski-Krastanov and Volmer-Weber modes (Figure 1.10). The growth mode is mainly determined by substrate-molecule and molecule-molecule interactions. Generally at the initial stages of growth a layer-by-layer growth is dominant due to the substrate interactions. When substrate

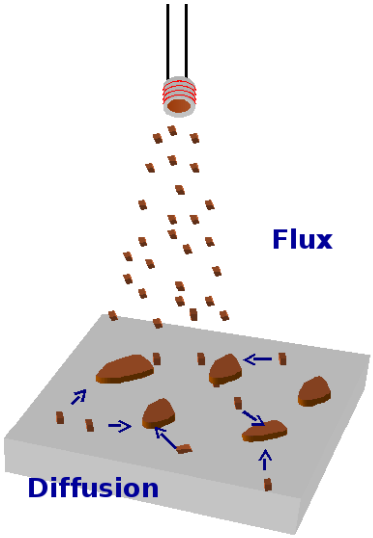

Figure 1.9: Shematic view of molecular beam deposition.

interactions are lowered after first few layers, island formations start to occur.

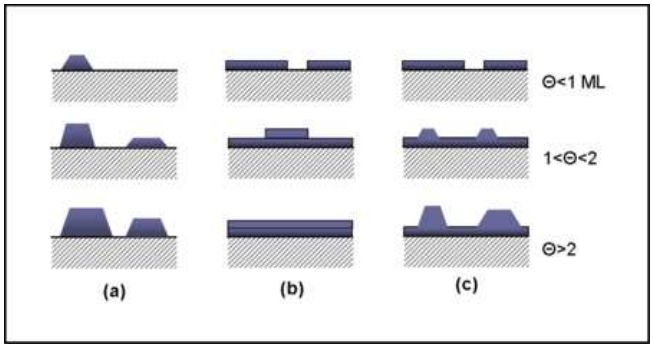

Figure 1.10: Common growth modes in thin film formation; (a) Volmer-Weber, (b) Frank-van der Merwe, (c) Stranski-Krastanov. Here Θ stands for the coverage.

Thin film morphology is also affected by film thickness [39]. Pesavento et al. observed increasing number of cracks on thin films by increasing film thickness. Also they have reported decrease in the mobility with increasing film thickness. Therefore the active layers corresponding to charge transport are also studied and believed to be the first few layers on the dielectric surface [40, 41].

1.4.2 Metal Surfaces

Another important issue is the electrode/semiconductor interface, which is relatively less studied and understood. According to SEM images of Dimitrakopoulos et al. [16] in Figure 1.11 it can be seen that the film morphology differs on the electrode surface from dielectric surface. Also film morphology changes at the interface between them.

Figure 1.11: Scanning electron microscopy (SEM) image of pentacene thin film grown on SiO_2 and Au [16].

Ihm et al. [42] studied the effect of molecular orientation on the hole injection barrier in pentacene thin films on the Au surface. They have used benzene, benzenethiol and methanethiol to modify the orientation of pentacene thin films, where pentacene oriented standing up on benzenethiol and methanethiol modified surfaces while lying down in methane modified and clean Au surfaces. They observed that hole injection barriers were lowered in the standing up orientation.

In most TFTs silver and gold are used as electrode materials and understanding the thin film growth of pentacene is very important to achieve better device performances. Hence, recent studies were focused on pentacene growth on different metal substrates both experimentaly [44, 45, 46, 47, 48, 49, 50, 51, 52, 53, 54, 55, 56, 57] and theoreticaly [58, 59, 60].

However these studies showed contradictory results for the growth of pentacene thin films on gold and siver surfaces, which is mostly due to the stronger interaction between pentacene and metal surfaces compared to SiO_2 surface. Because of this stronger interactions different monolayer and multilayer structures have been observed on these surfaces which are energetically and structurally close to each other. As an example, for Au(111) surface different low density monolayer structures have been reported in different studies with an identical full

monolayer structure [44, 45, 46, 47, 49]. Kang et al. [44, 45] reported four different monolayer structures with different densities in a room temperature growth and observed layer by layer growth of multilayers in lying down fashion with the same unit cell parameters of one of these monolayers. These ordered structures were found to be incommensurate with the Au(111) surface. However Beernink et al. [48] reported bulk like multilayers in an upright fashion on top of a lying down monolayer as islands. They reported strong dewetting starting from the second layer, and proposed that even STM tip can lead to removal of molecules. Lindstrom et al. [61] reported two distinct monolayer phase in a low temperature growth (90 K), one being low density and the other high density. For the low density phase they suggested lying down orientation for pentacene molecules. However, for the high density monolayer they suggested a tilted configuration due to weakening of the electronic coupling between adsorbed pentacene molecule and the metal surface in high density coverage than that of low density coverage. They observed also Stranski-Krastanov growth mode like Beernink et al. for multilayers. France et al. [47] observed four different structures in submonolayer regime and characterized two distinct monolayer phases at monolayer coverage. On Au(110) surface Floreanu et al. [56] also observed two distinct monolayer phase in the lying down fashion. For 370 K temperature they observed disordered growth while between 370 K and 420 K they observed bulk like multilayer islands.

On Ag(111) surface Eremtchenko et al. [53] reported a bilayer film formation at room temperature. They observed a disordered contact layer as a two dimensional gas phase on the surface. They found ordered second and third layers with same structure on the disordered contact layer (Figure 1.12).

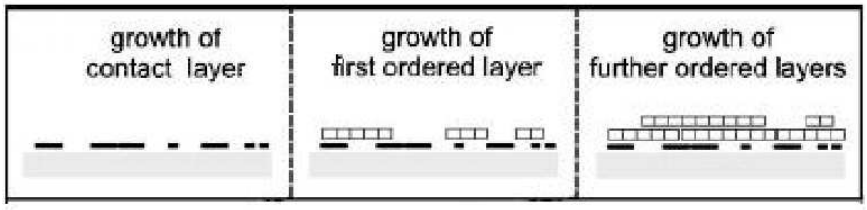

Figure 1.12: Bilayer growth of pentacene on Ag(111) surface proposed by Eremtchenko et al. [53].

The observed ordered layer has a unit cell of 8 ± 1 *Å* x 18 ± 1 *Å* and is tilted on the surface along the molecular long axis. They proposed that the nucleation of the ordered layers starts from the step edges of the Ag surface. Similarly Dougherty et al. [55] observed higly mobile pentacene molecules on Ag(111) surface with a room temperature growth and suggested the existance of a 2D gas phase. Upon cooling they have oserved two distinct monolayer phases with similar densities. The unit cells for these two structures was found to be 17 ± 2 *Å* x 8.5 ± 0.5*Å* with an angle of 60 ± 2° and 10 ± 1 *Å* x 15 ± 1 *Å* with an angle of 71 ± 2°. They also reported a bilayer film growth for pentacene on Ag(111) surface. In contrary Kafer et al. [50] reported bulk like multilayers with long molecular axis parallel to the surface in a room temperature growth. They observed a chemisorbed first layer tilted around the long molecular axis of pentacene. Danışman et al. [52] reported monolayer with a 6.1x3 surface unit cell for flat and stepped Ag(111) surfaces. However they observed ordered multilayers (Figure 1.13) only for the stepped surface. Film growth was done at low substrate temperatures by supersonic molecular beam deposition and ordered monolayers could be grown at 200 K via the effect of initial extra kinetic energy of molecules.

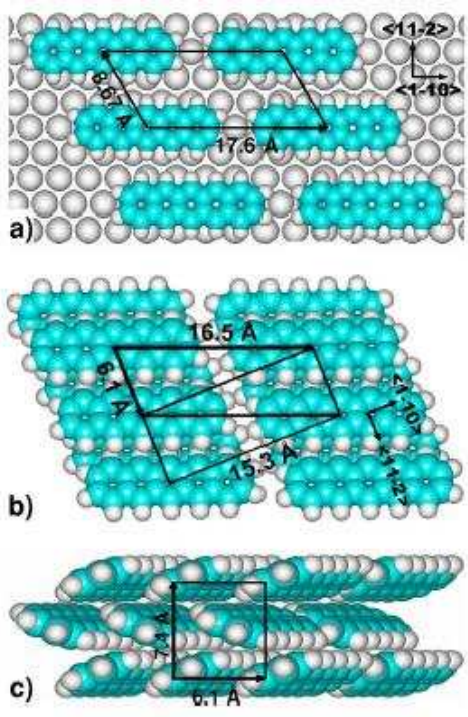

Figure 1.13: Model of the pentacene structures on Ag(111) surface [52]; (a) monolayer phase, (b) and (c) top and side views of multilayer phase respectively.

On Ag(110) surface Wang et al. [58] studied monolayer coverage for pentacene adsorption and found flat lying monolayer structure on the surface with the unit cell parameters 9.58 $\mathring{A}x16.59\ \mathring{A}$ with an angle of 125.3°. They also conducted molecular mechanic calculations and found flat lying down case is more favorable than the standing up orientations.

Although this debates can be clarified by theoretical studies, there is little work on pentacene on metal surfaces, even none on Ag(111) and Au(111). Theoretical studies performed on other metal surfaces are on Cu(001) [67], Cu(110) [62], Ag(110) [58] at semi empiric level and on Al(100) [63], Cu(100) [64], Cu(119) [65], Fe(100) [66], Au(001) [60, 59] at first principals level. These studies were mainly focused on the first layer of pentacene on these surfaces in the determination of the most stable adsorption site with adsorption geometry and determination of the electronic interaction between the surface and the molecule. In metal surfaces either a flat lying pentacene monolayer is found to be most stable [58] or calculations were started with this assumption. In a theoretical work Lee et al. [59] discussed the adsorption of a single pentacene molecule on Au(001) surface with DFT using LDA exchange correlation potentials. In their study they found the "bridge-b" (Figure 1.14) site with the angle 45° between long molecular axis of pentacene and substrate's [100] direction.

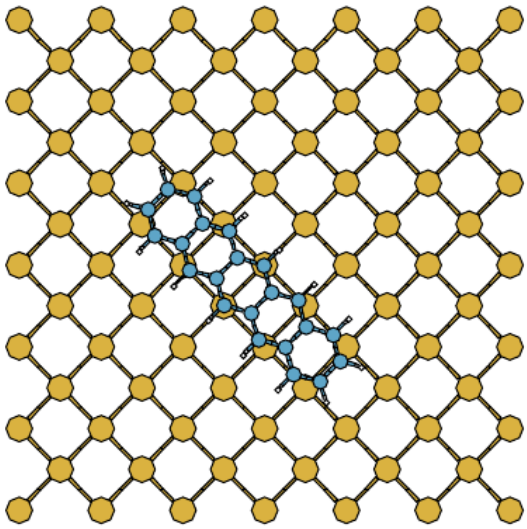

Figure 1.14: Bridge-b adsorption configuration of pentacene on Au(001) surface [59].

In this configuration pentacene carbon atoms follows the silver rows of (001) surface. They studied rotational and diffusion energy barriers on the surface and concluded with anisotropic

nature of the interaction between pentacene and surface. They found diffusion more favorable along long molecular axis than the other directions. They have also reported covalent bond formation between molecule and the surface. However in a later work [60] with different exchange-correlation potentials they observed that localized orbital methods and GGA types of exchange-correlation functionals give better results for the interaction between pentacene and silver surface in comparison with experimental results. For Cu surfaces DFT studies using GGA functionals found respectively strong pentacene-surface electronic interactions [64, 65] showing a chemisorption.Ample et al. [62] studied on Cu(110) surface by semiempirical methods and found also strong interaction between pentacene and surface. They also reported very high diffusion and rotational energy barriers. However on Au(001) [59] and Al(100) [63] while LDA functionals gave stronger interactions, GGA functionals resulted in weaker interactions, indicating physisorption. For the multilayers however, there are only few semi-empirical studies [67]. Most of the theoretical work concerning pentacene multilayers were on SiO2 surface instead [34, 25, 68, 69, 70]

Therefore a theoretical study of pentacene adsorption on Ag(111) and Au(111) surfaces may help to understand the interaction between pentacene and electrode interface, and may explain experimentally observed different monolayer and thin film structures, so that film growth can be optimized to obtain low charge injection barriers and high mobilities. In this regard we have started to investigate pentacene adsorption studies on Ag(111) surface. Since it is believed that the steps on the surface has an important role on ordered film growth [52, 53] we have continued with the interaction of the molecule with the stepped Ag(111) surface.

CHAPTER 2

METHOD

In this study we have performed density functional theory (DFT) calculations as implemented in the VASP (Vienna Ab-initio Simulation Package) code [71]. In this chapter a brief introduction to DFT and some concepts for the periodic structure calculations will be given.

2.1 Electronic Structure Calculations

2.1.1 Many-Body Schrodinger Equation

A theory for a stationary system of nuclei and interacting electrons is intrinsically quantum-mechanical, and is based on solving the time-independent Schrodinger equation of the form:

$$H\psi(\mathbf{R};\mathbf{r}) = E\psi(\mathbf{R};\mathbf{r}) \tag{2.1}$$

where H is the Hamiltonian of the system, containing the kinetic and potential energy operators; E is the energy of the system; ψ is the wavefunction of the system; [$\mathbf{R}$] are the positions of the nuclei, and [$\mathbf{r}$] are the variables that describe the coordinates of the electrons. The potential energy term arising from the repulsion of two electrons at $\mathbf{r}_i$,$\mathbf{r}_j$ is:

$$\frac{e^2}{|\mathbf{r_i} - \mathbf{r_j}|} \tag{2.2}$$

where e is the charge of an electron. The potential term arising from the attraction of an electron at $\mathbf{r}$ and a nucleus at $\mathbf{R}$ can be written as:

$$-\frac{Ze^2}{|\mathbf{R}-\mathbf{r}|} \tag{2.3}$$

where Z is the charge of the nucleus. The potential energy term for the repulsion of two nuclei can be written similarly:

$$\frac{Z_i Z_j e^2}{|\mathbf{R_i}-\mathbf{R_j}|} \tag{2.4}$$

For the kinetic energy of an electron the energy term will be:

$$-\frac{\hbar^2}{2m_e}\nabla_r^2 \tag{2.5}$$

Practically, it can be assumed that the nuclei move slower than the electrons, so that ψ has dependence only on the electronic degrees of freedom. This is called the Born-Oppenheimer approximation [72]. Its validity comes from the huge mass difference between nuclei and electrons, making the former behave like classical particles. So the term for the kinetical energy of the nuclei can be omitted and the repulsion term for the nuclei can be added as a constant contribution for specific atomic positions afterwards. In this case the Hamiltonian of the system becomes in atomic units:

$$H = -\sum_i \frac{1}{2}\nabla_{r_i}^2 - \sum_{iI}\frac{Z_I}{|\mathbf{R_I}-\mathbf{r_i}|} + \frac{1}{2}\sum_{i\neq j}\frac{1}{|\mathbf{r_i}-\mathbf{r_j}|} + \frac{1}{2}\sum_{I\neq J}\frac{Z_I Z_J}{|\mathbf{R_I}-\mathbf{R_J}|} \tag{2.6}$$

The last term in the previous equation is a constant and the electronic Hamiltonian can be written as:

$$H_e = -\sum_i \frac{1}{2}\nabla_{r_i}^2 - \sum_{iI}\frac{Z_I}{|\mathbf{R_I}-\mathbf{r_i}|} + \frac{1}{2}\sum_{i\neq j}\frac{1}{|\mathbf{r_i}-\mathbf{r_j}|} \tag{2.7}$$

Even with the proposed Born-Oppenheimer approximation, solving for $\psi(\mathbf{r})$ remains a difficult task, due to the many body nature of interactions. Each electron is affected by the motion of other electrons in the system, which is called correlation. Furthermore, two electrons of the same spin can change their positions, in which case ψ must change sign.

2.1.2 Density Functional Theory

Many-Body Schrodinger Equation is impracticle to solve for many electron systems. Therefore one should apply further methods to solve the problem. Density Functional Theory (DFT) provides a general framework to deal with the ground-state energy of the electrons in many-atom systems. DFT is based on two theorems, proved by Hohenberg and Kohn [73], and a computational scheme proposed by Kohn and Sham [74]. The first theorem states that the electronic structure of the ground state of a system is uniquely determined by the ground state electronic density, $\rho_0(\mathbf{r})$.The second theorem states a variational criterion for the determination of $\rho_0(\mathbf{r})$ and E_0 starting from an arbitrary function $\rho(\mathbf{r})$ constrained by the normalization condition:

$$\int d\mathbf{r}\rho(\mathbf{r}) = N \tag{2.8}$$

$$E[\rho] \geq E[\rho_0],\ E[\rho_0] = E_0 \tag{2.9}$$

where N is the total number of the electrons of the system. E_0 can therefore be found by minimizing with the method of Lagrange multipliers the functional $E[\rho]$ with respect to arbitrary infinitesimal changes in the form of the function $\rho(r)$. Kohn and Sham [74] showed that the ground-state density of the original interacting system is equal to that of some chosen non-interacting system. This leads to independent-particle equations for the non-interacting system that can be soluble, if all the difficult many-body terms are incorporated into an exchange-correlation functional of the density. For such a system the kinetic energy is defined as:

$$T_S = -\frac{1}{2}\sum_i \nabla_i^2 \tag{2.10}$$

This kinetic energy term forms part of the Hamiltonian operator that does not contain electron-electron interactions:

$$H_S = -\frac{1}{2}\sum_i \nabla_i^2 + \sum_i V_S(\mathbf{r_i}) \tag{2.11}$$

where $V_S(\mathbf{r})$ is an effective local potential. So the ground-state wavefunction associated with this Hamiltonian can be represented by a Slater determinant of the form:

$$\psi_S = \frac{1}{\sqrt{N!}} \begin{vmatrix} \varphi_1(x_1) & \varphi_1(x_2) & \cdots & \varphi_1(x_N) \\ \varphi_2(x_1) & \varphi_2(x_2) & \cdots & \varphi_2(x_N) \\ \vdots & \vdots & & \vdots \\ \varphi_N(x_1) & \varphi_N(x_2) & \cdots & \varphi_N(x_N) \end{vmatrix} \tag{2.12}$$

where the orbitals φ_i are termed Kohn-Sham orbitals. In this case the non-interacting kinetic energy is not equal to the interacting system's. Kohn and Sham accounted for that difference by defining the functional:

$$F[\rho(\mathbf{r})] = T_S[\rho(\mathbf{r})] + J[\rho(\mathbf{r})] + E_{XC}[\rho(\mathbf{r})] \tag{2.13}$$

where $J[\rho(\mathbf{r})]$ stems for the classical Coulomb integral of the electron-electron term and $E_{XC}[\rho(\mathbf{r})]$ is the exchange-correlation energy defined as:

$$E_{XC}[\rho] = (T[\rho] - T_S[\rho] + (E_{ee}[\rho] - J[\rho]) = T_C[\rho] + E_{ncl}[\rho] \tag{2.14}$$

The remaining part of the true kinetic energy, T_C is added to the non-classical electrostatic contributions, E_{ncl}. So everything that is unknown is contained in the exchange-correlation energy, which are the non-classical effects of self-interaction correction, exchange, correlation and a portion of the true kinetic energy. Thus, the total energy of the system can be expressed as:

$$E[\rho] = T_S[\rho] + J[\rho] + E_{XC}[\rho] \tag{2.15}$$

In this expression,the only term for wich no explicit form can be given is E_{XC}. If it were known, the exact ground-state energy could be found by solving the Kohn-Sham equations for independent particles. For an approximate form of E_{XC}, Kohn-Sham method provides a practical approach to calculating the ground-state properties.

2.1.3 Exchange-Correlation Functional

The important quantity in the Kohn-Sham method is the exchange−correlation energy, which is expressed as a functional of the density, $E_{XC}[\rho]$. In order to perform a precise DFT calculation, an accurate approximation to exchange-correlation functional is necessary. The first approximation to be suggested was the Local Density Approximation (LDA) [74]. The idea is to model the exchange-correlation of the actual system by using the properties of homogeneous electron gas:

$$E_{XC}^{LDA}[\rho] = \int dr \epsilon_{XC}(\mathbf{r}, \rho(\mathbf{r})) \tag{2.16}$$

where $\epsilon_{XC}[\rho]$ is the exchange-correlation energy per particle of a uniform electron gas with the same density of the system.

Although LDA works surprisingly better than predicted since it is a crude approximation, it is insufficient for the systems having inhomogenous density. In this sense the next approximation was made by the extension of exchange correlation energy in terms of the density [75]. In this approach only the density and its first derivative is included and the approximation is called Generalized Gradient Approximation(GGA):

$$E_{XC}^{GGA}[\rho] = \int dr f(\rho(\mathbf{r}), \nabla\rho(\mathbf{r})) \tag{2.17}$$

For choosing the function $f(\rho(\mathbf{r}), \nabla\rho(\mathbf{r}))$ there is no unique way, so that there exists many different GGA potentials. In general the GGA results are better than the LDA results, but this is not always the case. Thus it is useful to compare the results to have a more accurate result. In this study, two of the widely used GGA potentials, PW91 [76] and PBE [77] were used in addition to some LDA calculations.

2.1.4 Plane Waves

Solving the Kohn-Sham equations in real space is a difficult task. Instead some different basis sets are used to expand Kohn-Sham orbitals, such as pseudoatomic orbitals, plane waves etc. Plane waves are a good choice for basis sets in periodic systems, by their convenience in the

reciprocal space with Fourier transformations. For periodic systems the reciprocal unit cell is called Brilliouin zone and the infinitely many vectors spanning this space is called k-vectors. Since observables should be calculated by integrating over the Brilliouin zone one should take as many k-vectors as necessary in a numeric calculation to get accurate results, which is called k-point sampling. According to Bloch's Theorem [78], the wavefunction in a periodic system can be described by the product of a cell-periodic function, u(**r**,**k**), and a plane wave:

$$\phi(\mathbf{r}) = u(\mathbf{r}, \mathbf{k}) e^{i\mathbf{k}\cdot\mathbf{r}} \tag{2.18}$$

As any periodic function can be expanded in terms of plane waves, $u(\mathbf{r}, \mathbf{k})$ can be written as:

$$u(\mathbf{r}, \mathbf{k}) = \frac{1}{\sqrt{\Omega}} \sum_G c_i(\mathbf{k}, \mathbf{G}) e^{i\mathbf{G}\cdot\mathbf{r}} \tag{2.19}$$

where Ω is the volume of the unit cell and $c_i(\mathbf{k}, \mathbf{G})$ are the expansion coefficients. So the wavefunction will become:

$$\phi(r) = \phi_i(\mathbf{r}, \mathbf{k}) = \frac{1}{\sqrt{\Omega}} \sum_G c_i(\mathbf{k}, \mathbf{G}) e^{i(\mathbf{k}+\mathbf{G})\cdot\mathbf{r}} \tag{2.20}$$

By this way the Kohn-Sham equations are transformed from a set of differential equations into a set of algebraic equations. The expansion requires infinitely many G-vectors which is impossible to calculate. However this expansion can be truncated at some point, where for large G values, plane waves become negligible. This cut-off is called kinetic energy cut-off and denoted by E_{cut}.

2.1.5 Projector Augmented Wave Method

Finite plane wave expansions are insufficient in describing the strong oscillations of the wave functions near the nucleus and needs large number of plane waves for convergence and accuracy. Therefore some approximations are used. One of them is the pseudopotential method, which considers only the valence electrons and holds the core electrons to their behavior in a free atom. In the pseudopotiential approach, the Pauli repulsion of the core electrons is described by an effective potential that expels the valence electrons from the core region, causing

the wave functions to be smooth. However, all the information about the charge density and wavefunctions near the nucleus is lost [79]. Another type of approximation is the augmented wave method. In this method basis functions are composed of atom-like partial waves in the atomic regions and the bonding is appropriated by a set of functions. The space is divided by atom-centered spheres and an interstitial region for the bonds. The projector augmented wave (PAW) method is an extension of augmented wave methods and the pseudopotential approach, combining them into a unified electronic structure method [78]. In PAW method, space is considered as two but linked regions; interstitial and augmented regions. There is a transformation operator defined to transform highly oscillating all-electron wavefunctions to numerically convenient pseudowavefunctions. The transformation operater is choosen in a way that it only acts on the augmentation region. In the augmentation region, the wavefunction can be expanded in terms of the solutions for isolated atom. These solutions are called all-electron partial waves. In the intersititial region the solutions can be found by simply pseudopotential methods. At the end an all-electron wave function can be defined by combining these solutions by defined translation operator and projector operators [78].

2.1.6 Self-consisted Cycle

DFT calculations work within Kohn−Sham equations in a self-consistent manner. The calculations start with an initial guess for the charge density. By using this density the Kohn−Sham hamiltonian is constructed and solved for the Kohn−Sham eigenvalues and orbitals. By solving Kohn−Sham orbitals a new charge density is constructed and compared with the starting density. If they are not consistent the procedure repeats itself until the self consistency is achieved. This can be called electronic cycle and the tolerance for the convergence is given as a parameter in the calculations. For faster convergence in an electronic cycle, instead of using directly output density as an input in following step, some mixing shemes are used. For our calculations we used Broyden mixing sheme [80], which mixes the output density with previous input density to get the following input density. After the convergence for electronic cycle quantum-mechanical forces can be calculated on the atoms by using Hellmann−Feynman theorem [81]. To get the equilibrium positions for the atoms in the system, atoms are moved along these forces and the electronic cycles are repeated. Until the forces drop below a treshold value, the iteration cycle continues for the optimization of the geometry.

2.2 Hardware

Computations were performed by two computers with the specifications given in Table 2.1.

Table 2.1: Specifications of the hardware used through the study.

Name	CPU	Memory	Hard disk	Operating system
zirkon	8 * 2 GHz	8 GB	160 GB	Unix
titan	8 * 2 GHz	8 GB	160 GB	Unix

2.3 Software

Following computer programs were used to compute quantum mechanical calculations and to visualize the outputs throughout this study. These programs are:

- VASP

VASP is a package for performing ab-initio quantum-mechanical molecular dynamics (MD) using pseudopotentials and a plane wave basis set.

- XCrySDen

XCrySDen is a crystalline and molecular structure visualisation program, which aims as displaying the isosurfaces and contours, which can be superimposed on crystalline structures and interactively rotated and manipulated.

- Jmol

Jmol is an open-source Java viewer for chemical structures in 3D.

CHAPTER 3

RESULTS AND DISCUSSION

3.1 Bulk Silver

Bulk silver has a face centered cubic structure as shown in Figure 3.1 with $Fm\bar{3}m$ symmetry.

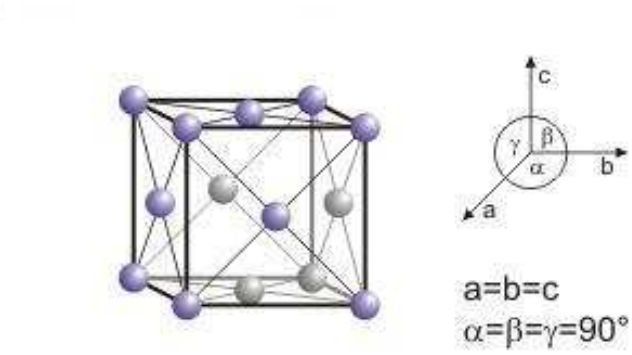

Figure 3.1: The conventional face centered cubic unit cell.

Lattice constant was calculated using three different exchange-correlation potentials which are LDA-PW91, GGA-PW91 and GGA-PBE. The results are listed in Table 3.1, and are consistent with the experimentally measured value [82] with small differences due to known properties of various exchange−correlation potentials. LDA potential resulted in 4.000 Å for the lattice constant with the largest deviation from the measured value. It is known that LDA underestimates bondlengths whereas GGA potentials underbind slightly [83]. In our case GGA-PW91 potential gave closer lattice constant to the experimental value than GGA-PBE potential. Even the GGA-PBE gave acceptable lattice constant which is closer to the

experimental value than the previously calculated value of 4.20 Å [84]. In further calculations these lattice constants are used according to used potential for constructing silver surfaces, since if experimental value is used the silver atoms will not be in their equilibrium positions in the unit cell.

Table 3.1: Lattice constant for silver crystal with different exchange−correlation potentials.

Potential	Lattice constant
LDA-PW91	4.000 Å
GGA-PW91	4.145 Å
GGA-PBE	4.173 Å
experiment [82]	4.090 Å

For this system we checked the energy convergence as functions of the type of k-point mesh (Figure 3.2) and the maximum kinetic energy, E_{cut} (Figure 3.3) value for the plane wave expansion.

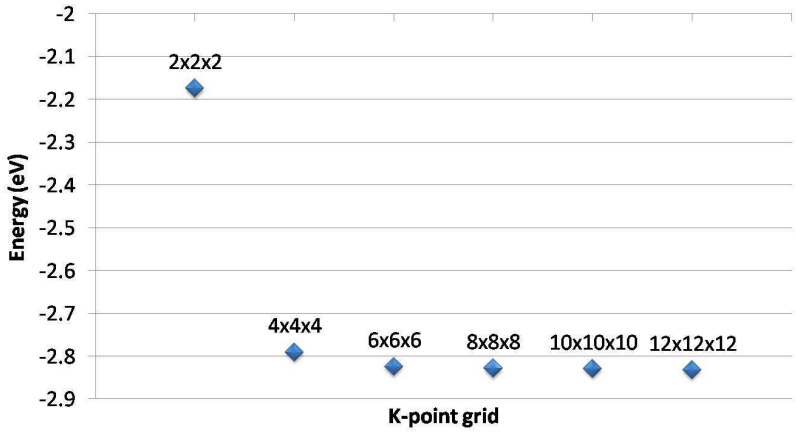

Figure 3.2: Energy convergence with respect to k-points in bulk Ag calculation.

It is important to optimize these values before carrying out larger calculations with more than 100 atoms in large unit cells. Because setting these values larger than enough will increase

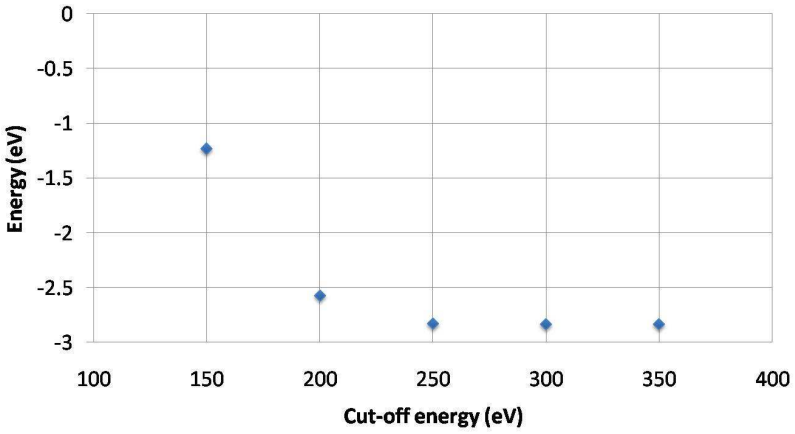

Figure 3.3: Energy convergence with respect to cut-off energy in Ag bulk calculation

calculation time and may make calculations impractical to perform due to large memory requirements. For Ag atoms an 250 eV cut-off energy is enough for energy convergence. As for k-point sampling, although the unit cell is small, after 6x6x6 grid the change in the energy is no longer significant.

3.2 Calculations for Pentacene Molecule

3.2.1 Isolated Pentacene

Pentacene structure was also studied with the use of different exchange–correlation potentials. The effect of k-points and cut-off energy selections for isolated pentacene molecule was also determined for further studies. The ground state of the molecule was checked within spin polarized calculations, whether it is singlet or triplet. Singlet ground state is found energetically more favorable as expected with 0.9 eV energy difference according to triplet state. Optimized geometry, atom positions and bond distances are given in Figure 3.4.

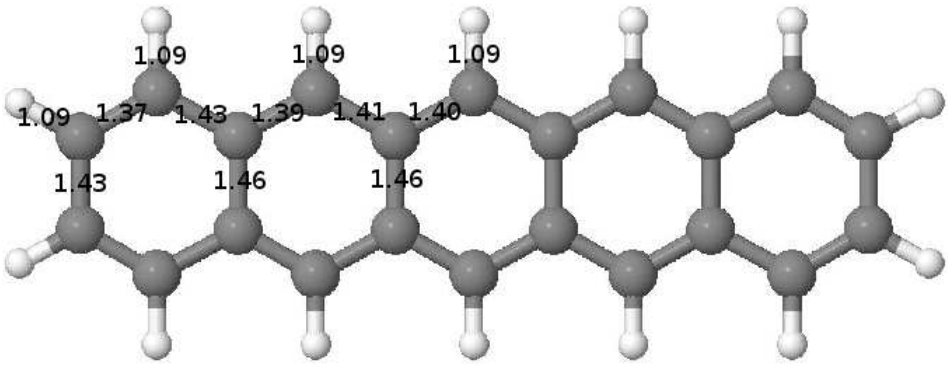

Figure 3.4: Isolated pentacene molecule. Symmetric bonds are found to have the same bondlengths as expected. Bondlengths are given in Å.

For three different exchange−correlation functionals (GGA-PBE, GGA-PW91, LDA-PW91) the same bondlengths was found for the pentacene molecule. Carbon−hydrogen bonds are found to be 1.09 Å. The hydrogen−hydrogen distances are found to be 14.13 Å along long molecular axis and 5.00 Å along short molecular axis. The molecule is found to be planar, and there is no significant deviation in the molecular plane. The bondlengths are found to be in good agreement with the experimental and previous theoretical results. The bondlengths differed at most 0.01 Å from the theoretical studies of Kadantsev et al. [85] and Endres et al. [24], and maximum 0.02 Å from the experimental value [22].

For this system total energy values did not show significant changes with respect to k-point grid (Figure 3.5). In further studies including both silver surface and adsorbed pentacene molecule, since more than 100 atoms will make a big system, consequently causing too much computer time and too much memory requirements, we limited our calculations within a 1x2x1 k-point sampling in adsorption calculations owing to large unit cell dimensions and this small energy differences. In solid pentacene calculations however, we have the option to include more k-points in our calculations. A 4x6x3 grid was used in these calculations to obtain a uniform distribution of k-points in the unit cell. For plane wave expansions a cut off of 300 eV is found to be sufficient to simulate pentacene molecule (Figure 3.6). For accuracy

a 370 eV cut-off energy is chosen and used in all of the following computations.

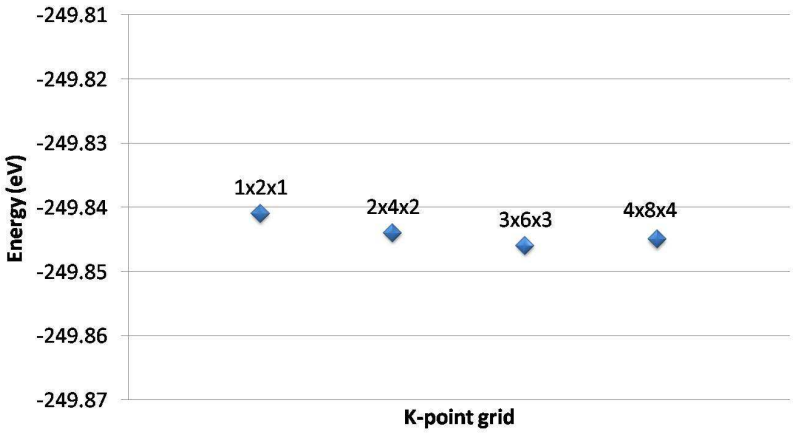

Figure 3.5: Energy convergence with respect to k-points for isolated pentacene calculation.

Table 3.2: Total energy values for isolated pentacene system with different exchange−correlation potentials.

XC potential	Total energy	Fermi energy	HOMO−LUMO gap
LDA-PW91	−250.450 eV	−3.874 eV	1.141 eV
GGA-PW91	−250.455 eV	−3.906 eV	1.141 eV
GGA-PBE	−249.784 eV	−3.659 eV	1.137 eV

The energies were found to be slightly different with different exchange−correlation functionals (Table 3.2). For GGA-PW91 and LDA-PW91 total energy values are very similar but for GGA-PBE there is larger energy difference. Since these values are used only for the calculation of adsorption energies, i.e. only the relative energies will be discussed for the same exchange correlation functionals, these differences are not important. HOMO−LUMO gap is calculated from the Kohn−Sham eigenvalue differences. For HOMO−LUMO gap all the potentials gave very close results with respect to each other and with respect to previous theoretical calculations, but very different from the experimental value. Endres et al. [24] found 1.1 eV for HOMO−LUMO gap depicted by eigenvalue differences in a previous thoretical

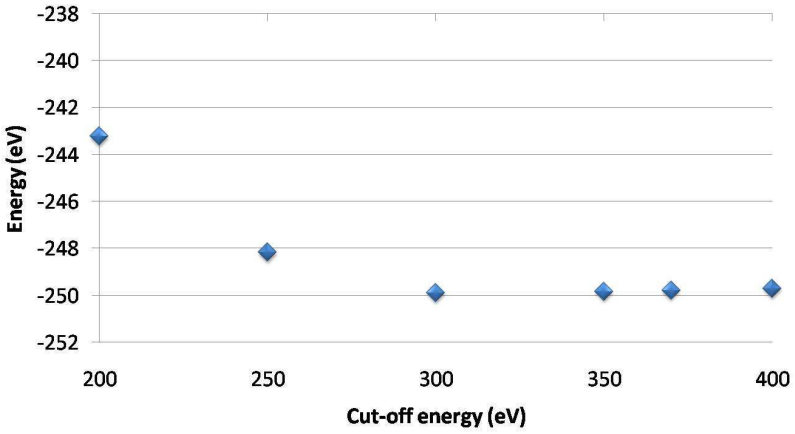

Figure 3.6: Energy convergence with respect to cut-off energy for pentacene in a box calculation.

work, whereas the experimental value is 5.22 eV in the gas phase [86]. This underestimation of HOMO−LUMO gap is a common deficieny of DFT calculations due to the discontinuity of exchange−correlation functionals with respect to the number of electrons [87]. DFT is known as a groundstate theory and deficient for unoccuppied states. Hence better estimation for HOMO−LUMO gap, Δ, can be made by total energy differences [88]:

$$\Delta = E_0(N+1) + E_0(N-1) - 2E_0(N) \tag{3.1}$$

where $E_0(N)$ is the groundstate total energy of the neutral N electron system and $E_0(N \mp +1)$ is the groundstate total energy of one electron added/removed system with the same geometry. By this method 4.31 eV HOMO−LUMO gap was found for GGA-PBE potential which is an improvement to the previous value of 1.14 eV and closer to the experimental value of 5.22 eV.

3.2.2 Solid Pentacene

For pentacene bulk structures, three different polymorphs were investigated. These are bulk phase and experimentally observed thin film phases on SiO_2 [25] and Ag(111) [52] surfaces. Bulk lattice parameters are taken from Campbell's work [22] which are listed in Table 3.3. Bulk phase corresponds to a triclinic unit cell containing two pentacene molecules tilted with respect to each other Thin film phases are bulk like structures preserving the herringbone structure of bulk phase, with different lattice parameters. Thin films on SiO_2 were reported to have an orthorombic unit cell, and parameters were taken from Parisse et al. [25] for our calculations. Lastly we have calculated total energy for the thin film phase grown on Ag (111) surface by Danışman et al. [52]. This phase corresponds to monoclinic unit cell with parameters given in Table 3.3.

Table 3.3: Lattice parameters for pentacene structures.

Phase	a (Å)	b (Å)	c (Å)	α (deg)	β (deg)	γ (deg)
Bulk [22]	7.90	6.06	16.01	101.9	112.6	85.8
Thin film (SiO_2) [25]	7.6	5.9	15.43	90	90	90
Thin film (Ag) [52]	7.40	6.16	16.02	68.9	90	90

We have conducted pentacene solid calculations within a 4x6x3 k-points sampling with an 370 eV cut-off energy. We used GGA-PBE potential for this calculations because LDA gave unreasonable results in pentacene adsorption on Au(001) surface [60] among other used potentials. The energy values are given in Table 3.4. It is obvious that bulk phase will be the most stable one among other polymorphs but there are energetically small differences among these structures, which can be facilitated with the adsorption energies. There is only 76 meV energy difference between the pentacene polymorph observed on Ag(111) surface and the bulk phase.

Table 3.4: Calculated total energies for different pentacene polymorphs.

Phase	Unit cell	E (eV)	E_{rel} (eV)
bulk	triclinic	−499.388	0.000
thin film (SiO_2)	orthorombic	−499.270	0.118
thin film (Ag)	monoclinic	−499.312	0.076

3.3 Single Pentacene on Ag(111)

To study the adsorption site of pentacene on Ag(111) surface a single molecule was investigated on the surface. To isolate molecule on the surface a large unit cell was chosen, for which there is no interaction between neighboring pentacene units in the periodic structure. In this manner we have made use of Lee's work [59], in which they calculated the interaction between two pentacene molecules. They have calculated side by side and head to head interactions and found equilibrium distances. According to their work there is no energy difference beyond 8 Å for side by side and 17 Å for head to head configurations. Therefore, an even larger unit cell with dimensions 14.7 Å and 20.6 Å was chosen (Figure 3.7). There are 141 atoms in this unit cell.

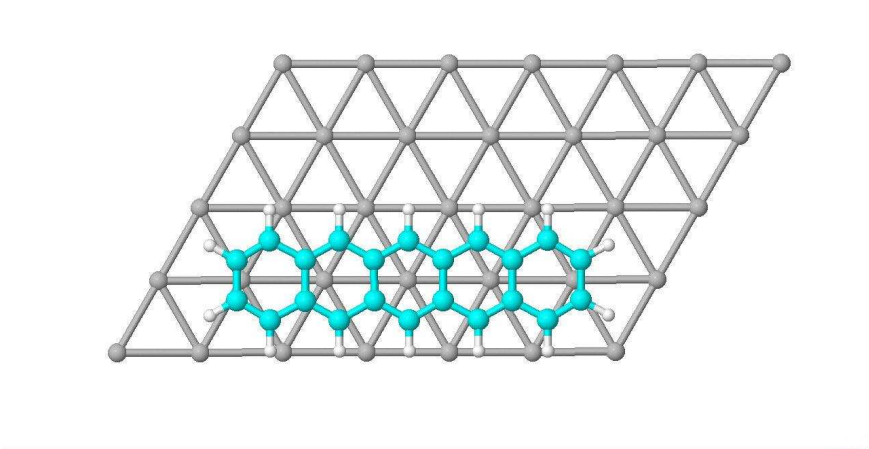

Figure 3.7: Surface unit cell with pentacene molecule.

In a cubic close packed (111) surface there are mainly three adsorption sites, which are top (on top of a surface atom), bridge (between two surface atoms) and two hollow (midpoint between three neighboring surface atoms) sites (Figure 3.8). The difference in the hollow sites is due whether there is an atom in the second layer or not.

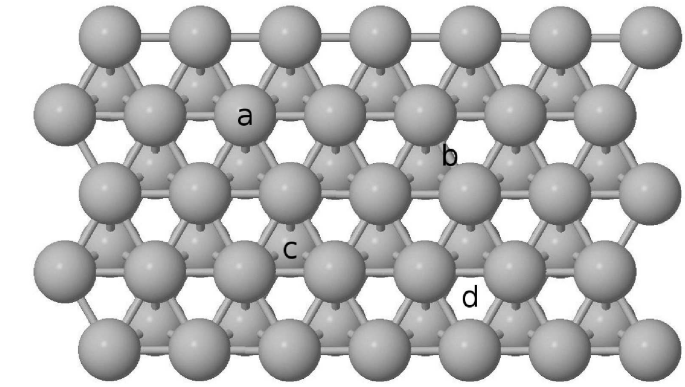

Figure 3.8: Adsorption sites for a fcc(111) surface; top site “a”, bridge site “b”, and hollow sites “c” and “d”.

To simulate silver surface, three and four-layer slabs was studied without the adsorbate. In these calculations there was not significant changes in both the positions and the forces on silver atoms. When the weak interaction between pentacene molecule and silver surface was taken into account, 3-layer slab (Figure 3.9) was found to be enough to simulate the silver surface due to very small distortions on the atomic positions.

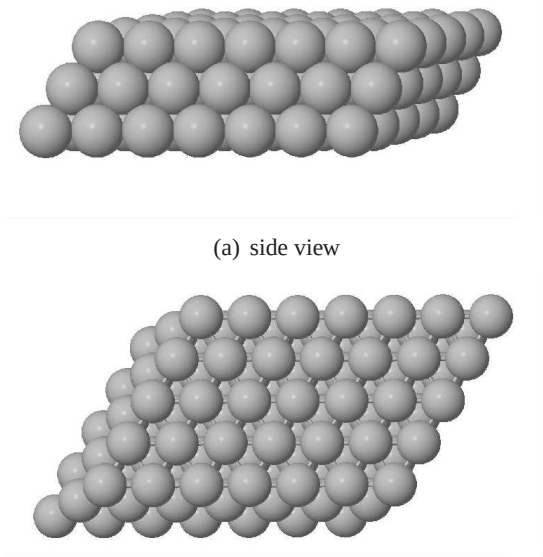

(a) side view

(b) top view

Figure 3.9: Three layer surface slab of Ag surface.

We have denoted adsorption configurations with respect to the molecular center of pentacene.

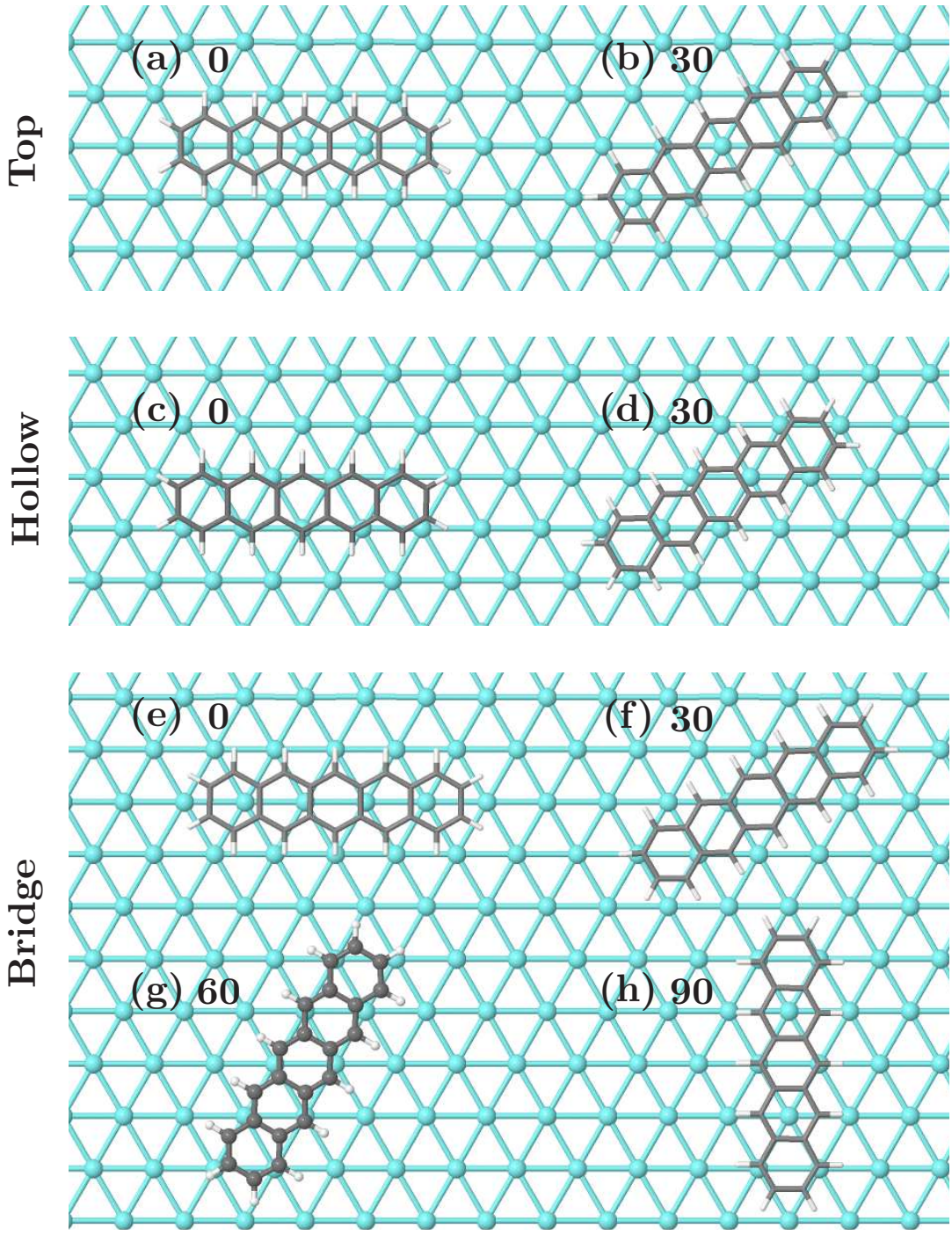

Figure 3.10: Single isolated pentacene on different adsorption sites of Ag(111) surface; (a) top-0, (b) top-30, (c) hollow-0, (d) hollow-30, (e) bridge-0, (f) bridge-30, (g) bridge-60, (h) bridge-90. All in wireframe except the lowest-energy case of (g) which is shown in ball-and-stick mode.

We have selected 8 possible adsorption configurations in our case according to the symmetry of the system. We abbreviated these configurations with the name of the site and the angle between long molecular axis of pentacene and the $[0\bar{1}1]$ direction of metal surface. In all the configurations pentacene lies flat on the surface. These configurations are top-0, top-30, hollow-0, hollow-30, bridge-0, bridge-30, bridge-60 and bridge-90 as shown in Figure 3.10. For top and hollow configurations 60 and 90 degree rotations are identical with 0 and 30 degree rotations, respectively, due to the hexagonal surface symmetry.

In geometry optimizations we have determined the adsorption heights (d_z) and corresponding binding energies. Binding energies (E_b) are calculated with the following formula [88]:

$$E_b = E_{sys} - E_{sur} - E_{mol} \tag{3.2}$$

where E_{sys} is the energy of the full system, E_{sur} and E_{mol} are the energies of surface and the molecule seperately. All the adsorption configuration calculations were conducted within GGA-PBE exchange−correlation functional and only the most favorable case, bridge-60, was repeated with GGA-PW91 functional. The results for the adsorption configurations are given in Table 3.5. E_{rel} is the relative energies according to the lowest energy configuration, in our case bridge-60. For bridge-60 binding energy, being the strongest among all, is found to be -0.155 eV. It corresponds to a physisorption on the surface with negligible disturbance in the flatness of pentacene molecule. Corresponding adsorption height is found to be 3.87 Å.

Table 3.5: Calculated values for geometrical and electronic structure of Pn/Ag(111) configurations shown in Figure 3.10. The lateral height of isolated Pn molecule from the Ag(111) surface d_z in Å, the binding energy E_b and the relative total energy E_{rel} in eV.

Configuration	d_z (Å)	E_b (eV)	E_{rel} (eV)
Top-0	3.90	−0.125	0.030
Top-30	3.89	−0.119	0.036
Hollow-0	3.88	−0.147	0.008
Hollow-30	3.87	−0.128	0.027
Bridge-0	3.87	−0.124	0.031
Bridge-30	3.88	−0.124	0.031
Bridge-60	3.87	−0.155	0.000
Bridge-90	3.88	−0.129	0.026

Two different hollow sites were included in calculations but the energies did not change as

expected within the tolerance value, so only one hollow site is given in the results. This also implies that only the first layer of surface involves in the interaction with pentacene molecule. Hence, three layer surface slab is enough to simulate the interface. By examining the relative energies one can conclude the existence of a flat potential energy surface for the pentacene molecule on the surface. There are no more than 36 meV energy differences between these configurations. These small energy differences also indicate small diffusion barriers for pentacene molecule on the surface. These small barriers are in agreement with the experimental observations of Eremtchenko et al. [53] and Dougherty et al. [55], in which the contact pentacene layer was mobile at the interface.

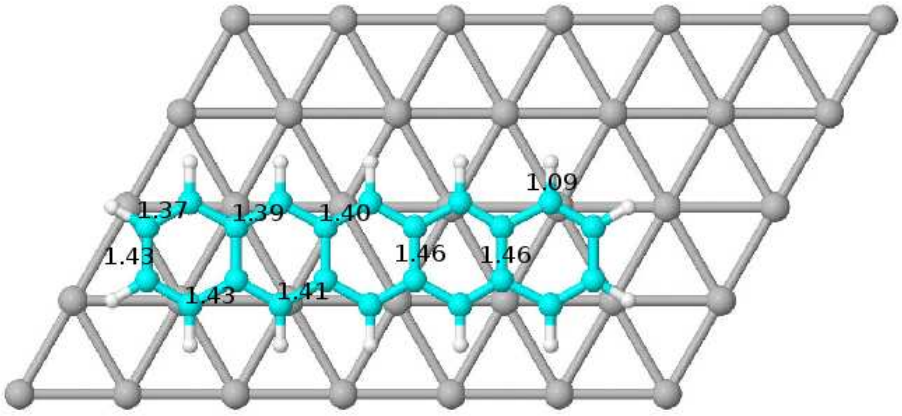

Figure 3.11: Bridge-60 configuration. Bondlengths are given in Å.

The adsorption configurations, in which carbon−carbon bonds folows the silver lattice on the surface, were found to be energetically more favorable. For example bridge-60 and hollow-0 configurations were found to give maximum adsorption energy, −0.155 eV and −0.147 eV, respectively. Also the least favorable configuration was found to be top-30 with −0.119 eV adsorption energy, mostly due to three ring of pentacene not seeing any silver atom or silver−silver bond of the surface layer, i.e. there is only 4 top interaction between π delocalized carbon−carbon system and surface silver atoms. In Bridge-90 configuration, however,

improvement on the adsorption energy can be seen due to 6 top interaction. Bridge-90 configuration was found to give -0.129 eV adsorption energy. Similarly hollow-30 configuration gave nearly same adsorption energy with bridge-90, -0.128 eV, following the same trend. In hollow-30 configuration there is more top interaction than bridge-60, but all of them are slighty deviated from being head to head interactions. Furthermore, for favorable bridge-60 and hollow-0 configurations two carbon rows at long molecular axis of pentacene follows the silver lattice very closely giving maximum interaction. However, in top-0 and bridge-0 these two rows are between silver rows at $[0\bar{1}1]$ lattice direction which result in less interaction ~ -0.125 eV. Hence, the interaction between surface silver atoms and the carbon$-$carbon delocalized system determines the adsorption energy and the flatness of potential energy surface can be said to be stronger for lattice directions of silver surface. Therefore, it can be said that where the pentacene molecule follows the lattice symmetry so that the molecular charge density can overlap effectively with the surface charge density of silver rows are energetically more favorable. Similar observations was also made for pentacene adsorption on Au(001) [59] and Cu(110) [62] surfaces, where pentacene prefers to align according to surface atom rows.

In Figure 3.11 the bond lengths of pentacene molecule on the silver surface are given. These values are exactly the same as the isolated pentacene molecule which shows that there is no molecular distortion on pentacene molecule on the surface. Together with small adsorption energies, this indicates that there is not a chemical bond formation between pentacene molecule and the silver surface. Also by considering the covalent bond radius and Van der Waals radius of silver and pentacene carbon atoms one should expect 2.18 Å adsorption height for covalent interaction and 3.42 Å for Van der Waals interaction. Calculated 3.90 Å for GGA-PBE and 3.69 Å for GGA-PW91 adsorption heights indicates that there is physisorption by weak van der Waals interactions. This is not an agreement with the proposed chemisorption by Kafer et al. [50], however a good agreement with loosely bound contact layer of Eremtchenko et al. [53].

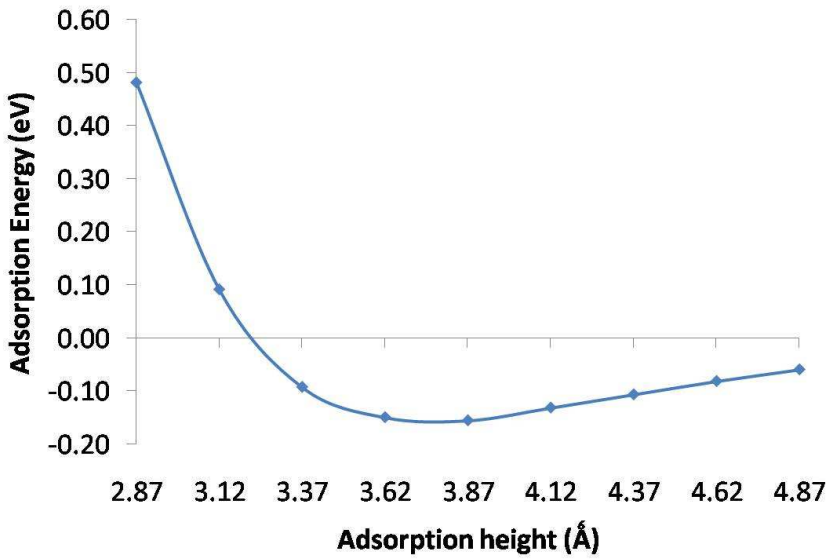

(a) GGA-PBE

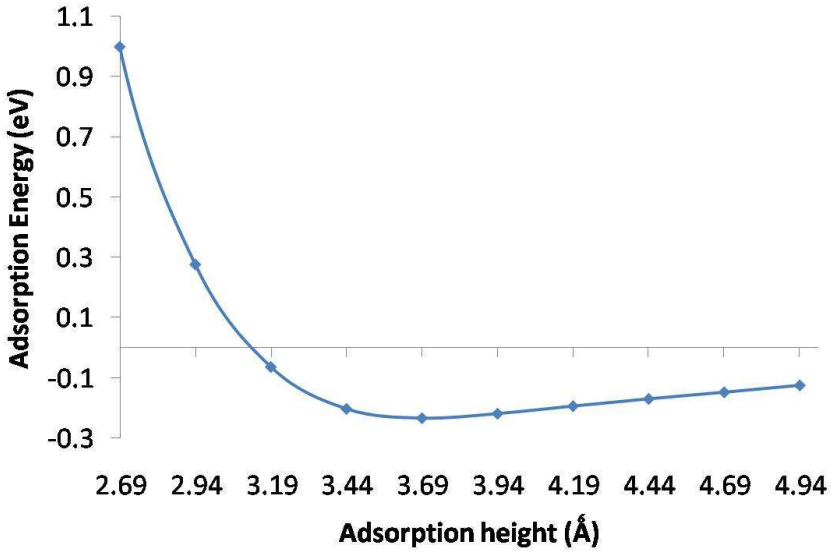

(b) GGA-PW91

Figure 3.12: Energy versus adsorption height for bridge-60 configuration (a) with GGA-PBE and (b) with GGA-PW91.

Nearly the same adsorption heights about 3.9 Å were found for all the configurations using GGA-PBE functional. The energy change with respect to adsorption height for bridge-60 configuration is given in Figure 3.12 for GGA-PBE and GGA-PW91 functionals.

3.3.1 Diffusion on surface

By looking at the adsorption enegy differences in different adsorption configurations, one can comment on the diffusion tendency of pentacene molecule on the surface. Although the differences could not be said to represent the diffusion barriers exactly without investigating all the paths between different sites, they can still give relative idea about diffusion directions. There is also a similar study by Lee et al. [59] extracting diffusion barriers calculated in the same way on Au(001) surface with LDA functional, giving both rotational and diffusion energy barriers. For the rotation on a bridge site we have found rotation barriers around 31 meV (Figure 3.13).

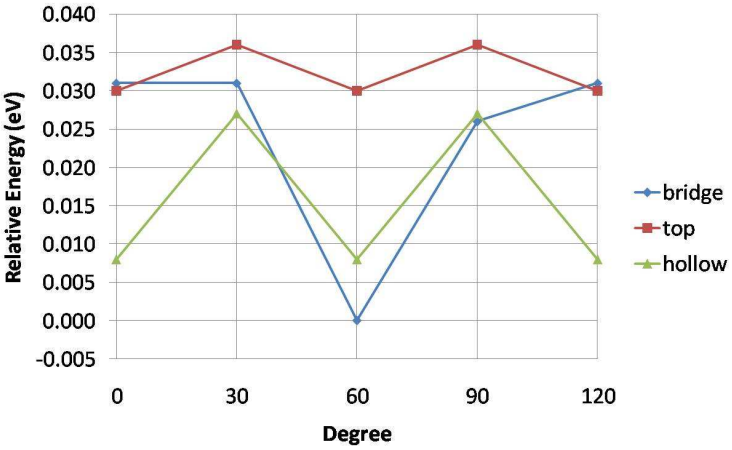

Figure 3.13: Energies with respect to rotation of the molecule on adsorption site.

For hollow and top sites since 60 and 90-degree configurations are equivalent to 0 and 30-degree respectively, no new calculations were performed. In energeticaly second favorable hollow site, where pentacene molecule follows silver rows similar as bridge-60 rotational energy barrier seems lowered to 19 meV. Furthermore, for the least favorable site, top site, the rotational energy barrier seems as low as 6 meV. Diffusion energy barriers were also found to be very low. In Figure 3.14 the longest path between two bridge-60 configurations is given along $[2\overline{11}]$ direction.

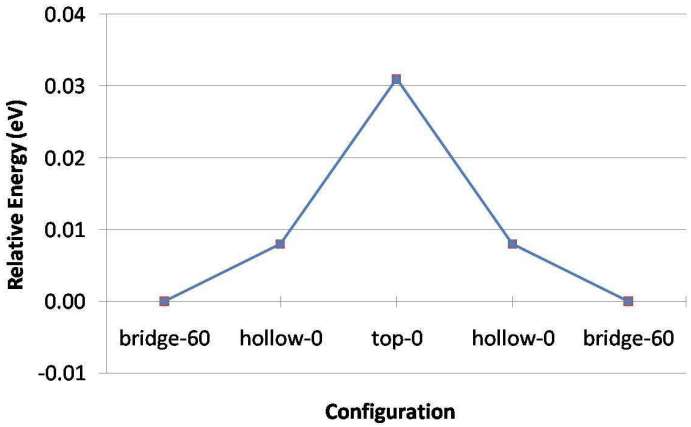

Figure 3.14: Diffusion path between two bridge-60 configuration.

The diffusion energy barrier seems to be around 30 meV in this direction. For diffusion along long molecular axis of pentacene diffusion energy barriers seems to be even lowered, 8 meV for a diffusion between two bridge sites if we assume path includes hollow-0 configuration. For this very short path we have studied also the configuration where molecular center of pentacene was placed the mid point of two bridge-60 configuration and it is found energeticaly more favorable than hollow-0 site by 2 meV. Diffusion perpendicular to molecular long axis of pentacene was found as 30 meV. Along with the energy differences in other configurations it seems that diffusion along long molecular axis of pentacene is more favorable. Similar observation were made by Lee et al. [59] on Au(001) surface. Although they found higher rotation and diffusion barriers between 0.45 and 1.26 eV, they also indicated lower diffusion barriers along long molecular axis of pentacene. These larger barriers can be attributed to the more reactive surface (001). In our case the rotational and diffusion energy barriers do not seem to surpass 40 meV. Hence an oncoming pentacene molecule can easily diffuse on the surface and can find a favorable position. Although 40 meV is a very low energy barrier, it is not as low as that the diffusion can be said to be independent of the temperature in the range of substrate temperatures in the pentacene film growth. The relation between diffusion coefficient and the temperature for surface diffusion can be given as [89]:

$$D = D_0 e^{-E/kT} \tag{3.3}$$

where D is the diffusion coefficient, D_0 is the diffusion coefficient at the limit of infinite temperature, E is the activation energy of diffusion and k is the boltzman constant. In our case, the energy differences of $\sim$ 40 meV indicate that diffusion coefficient increases by a factor of 2 with an increase in temperature to 200 °C from room temperature which is in the range of the substrate temperatures during pentacene thin film growth. Hence, controlling the diffusion plays an important role in the ordered film formation, since the binding energy, 155 meV, is also not too high when compared with the diffusion barriers. Diffusion energy barriers lower than kT indicates physisorption as well as 2-dimensional gas phase on a surface [90], which is the case for our system. This agrees with the experimentally observed disordered gas phase contact layer of pentacene on Ag(111) surface by Eremtchenko et al. [53].

3.4 Monolayer coverage

In experimental studies on Ag(111) surface [52, 55, 51] a common monolayer phase was found stable beside some different low coverage phases. The surface unit cell dimensions for these observed monolayer phases are given in Table 3.6. These phases fit in a 6x3 surface unit cell for calculated silver lattice constants of GGA-PBE and GGA-PW91.

Table 3.6: Monolayer lattice parameters for pentacene on Ag(111).

	a (Å)	b (Å)	α (deg)
Danisman et al. [52]	8.67	17.6	60
Dougherty et al. [55]	8.5	17.0	60
GGA-PBE	8.85	17.59	60
GGA-PW91	8.79	17.71	60

Before the adsorption calculations, pentacene was calculated inside this surface unit cell without silver surface. The resulted geometry (Figure 3.15) showed no difference with isolated pentacene calculation, and for energetics (Table 3.7) the values are very close to each other.

Calculations than continued with the creation of the silver surface. For monolayer study a 6×3 surface unit cell was used with 4 layer slab. A 15 Å vacuum was used to seperate these slabs from each other in z direction. Flat pentacene molecule was placed on a bridge-60 configuration which is found more favorable in previous calculations. There are 108 atoms

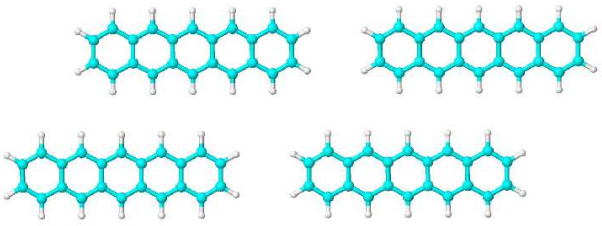

Figure 3.15: Pentacene monolayer structure.

Table 3.7: Total energy values for isolated pentacene and monolayer phase for GGA-PBE potential.

	a (Å)	b (Å)	α (deg)	Total energy
Isolated pentacene	18.0	25.0	90	−249.784 eV
Monolayer pentacene	8.85	17.71	60	−249.837 eV

in the unit cell. The calculated energies are listed in Table 3.8 in addition to the results for isolated monolayer case for comparison.

Table 3.8: Calculated values for electronic and geometrical structure of Ag and Pn/Ag(111) systems in different exchange–correlation functionals. Lattice parameter of Ag(111) slab a_{Ag} in Å, lateral heights d_z (Å) and the binding energies E_b (eV) of isolated and 1 ML Pn on the Ag(111) surface.

	Clean slab	Isolated Pn		1 ML Pn	
	a_{Ag}	d_z	E_b	d_z	E_b
GGA-PW91	4.145	3.69	−0.234	3.94	−0.093
GGA-PBE	4.174	3.87	−0.155	4.12	−0.078

Similar to the isolated case, monolayer phase of pentacene was found without any distortion on the molecule. Adsorption energies were lower for both GGA-PW91 and GGA-PBE functionals. Accordingly the adsorption heights were extended, 4.12 Å for GGA-PBE and 3.94 Å for GGA-PW91 functional. This is mainly due to the pentacene pentacene interactions. At this point one can say that adsorption height varies with intermolecular interaction strength.

With the weaker interaction between pentacene and surface in the monolayer coverage, physisorption gains more evidence for pentacene adsorption.

3.5 Pentacene on stepped Ag(111) surface

3.5.1 Ag(233) surface

Previous experimental studies showed that steps on the silver surface have an important effect on the ordered pentacene film growth [52, 53]. To understand the effect of steps on pentacene adsorption, the interaction between pentacene and stepped Ag(111) surface was studied. Ag(233) surface was chosen in these simulations due to its stability [91]. Ag(233) surface (Figure 3.16) has (111) steps and (111) terraces with 6 silver atom rows. 7x6 surface unit cell was chosen with 3 layer slab to isolate pentacene molecule on the surface. There are two different types of silver atoms on Ag(233) surface; first being the high coordinated atoms and the other low coordinated. The angle between the terrace and the step (θ) is 109.5° and the step angle is 10°. Surface relaxations mainly took place for the atoms around the step. Low coordinated silver atoms got closer to other silver atoms, while high coordinated ones moved slightly outwards to the surface. Besides these relaxations other silver atoms did not show significant changes in terms of atomic positions.

On the Ag(233) step pentacene was placed as its long molecular axis paralel to the step. Initial calculations were started to find the minimum energy configuration of pentacene on the surface. To find the lowest energy configuration, different adsorption geometries were calculated as single point calculations. In this configurations molecular center of pantacene was placed at a distance from the high and low coordinated silver atoms with the angle of $\theta/2$. For comparison, flat configurations of pentacene on the silver terrace far from the step were also studied. The calculated geometries and the labeling are given in Figure 3.17.

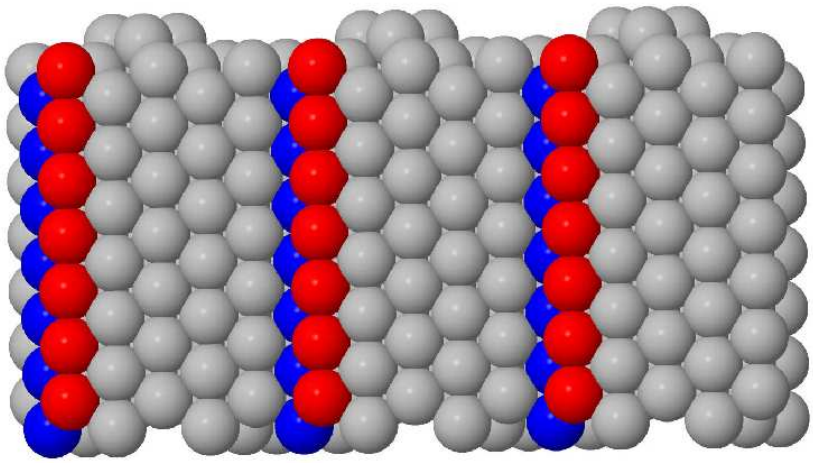

(a) top view

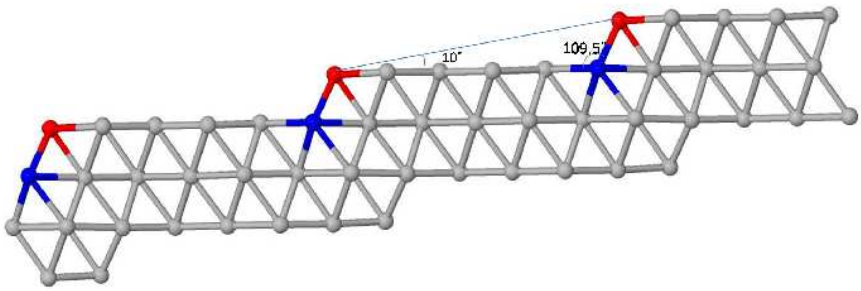

(b) side view

Figure 3.16: Ag(233) surface. High and low coordinated silver atoms are highlighted with blue and red colors, respectively.

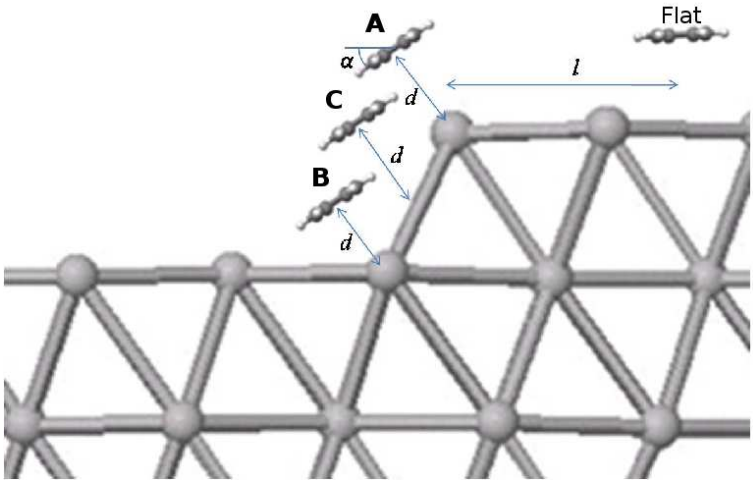

Figure 3.17: Labeling for adsorption geometries of pentacene on Ag(233) surface. Pentacene icons are not drawn to scale.

For these adsorption geometries, energy differences with respect to distance (d) and angle (α) were calculated and listed in Table 3.9. In this calculations GGA-PW91 exchange–correlation functional was used because it gave better results for isolated and monolayer cases on Ag(111) surface. GGA-PW91 results lied between GGA-PBE and LDA-PW91 results, where we think the exact result should find its place. A 1x2x1 k-point grid was used with 370 eV energy cut-off.

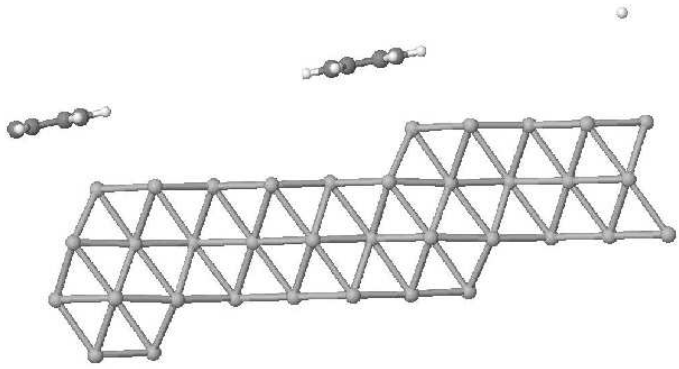

Figure 3.18: Minimum-energy configuration for the adsorption geometry A.

Table 3.9: Relative energy values, E_{rel}, for different adsorption geometries calculated as single point calculations.

Geometry	d (Å)	α (°)	E_{rel} (eV)
A	3.5	0	0.183
	3.5	10	0.162
	3.5	15	0.142
	3.5	20	0.120
	3.5	25	0.101
	3.5	30	0.104
	3.5	45	0.412
B	4.7	0	0.498
	5.1	0	0.322
	5.1	10	0.229
	5.3	10	0.236
	5.5	0	0.282
	5.5	10	0.247
	5.5	20	0.253
C	4.1	0	0.137
	4.1	10	0.029
	4.1	**15**	**0.000**
	4.1	20	0.006
	4.1	30	0.176

At first glance, it can be seen that for the configurations where pentacene molecule interacts with the step atoms, i.e. pentacene molecule is close to the low coordinated step atoms, total energy is lowered. Among these three geometries, for the configuration A, the minimum-energy geometry was found with the distance, d = 3.5 Å with the angle, α = 25° (Figure 3.18). The angle between molecular plane and the surface plane (233) is found to be 0.3°. In this configuration the pentacene molecule is close to the step atoms, ~ 3.2 Å, however far from the terrace atoms, ~ 4.7 Å. In configuration B where pentacene molecule is more into the step edge than A, the distance between pentacene molecule and the terrace is lowered to 3.65 Å, which is the distance for an isolated molecule on the flat (111) surface. However, the total energy did not improve. This is probably because in this case carbon π system loses its direct interaction with the low coordinated step atoms geometrically (Figure 3.19). For this configuration the angle between the surface plane (233) and the molecular plane is found to be 15.2°.

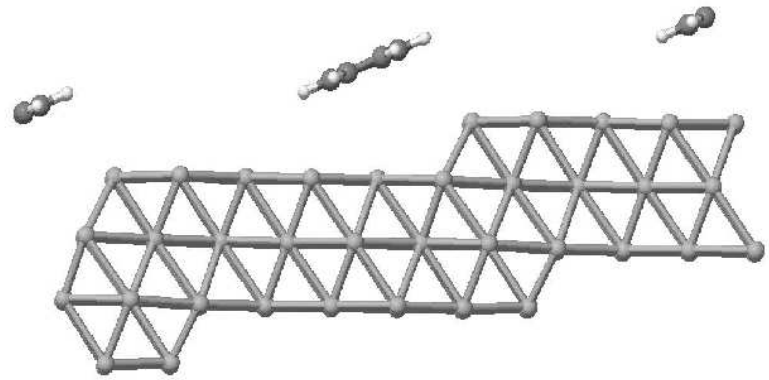

Figure 3.19: Minimum-energy configuration for the adsorption geometry B.

The minimum energy was found for the geometry C which stands between A and B cases, where the molecule can interact with step atoms without losing its contact with the terrace. In this configuration there is 3.00 Å between pentacene molecule and the low coordinated silver surface atoms while the distance of molecule to the terrace is ~ 3.75 Å (Figure 3.20). The angle between surface plane and molacular plane was found to be 7°, which is in between A and B geometries.

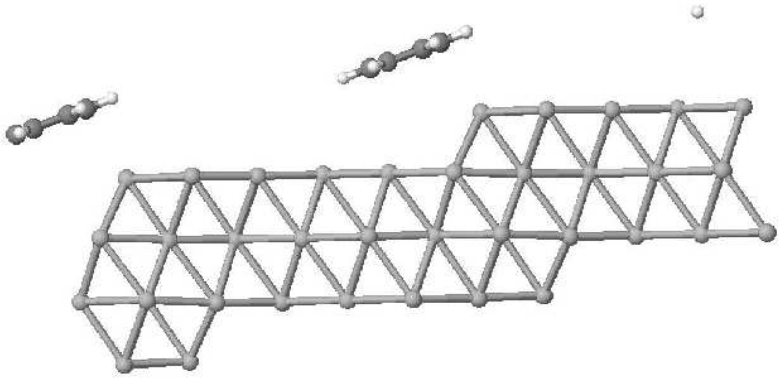

Figure 3.20: Minimum energy configuration for the adsorption geometry C.

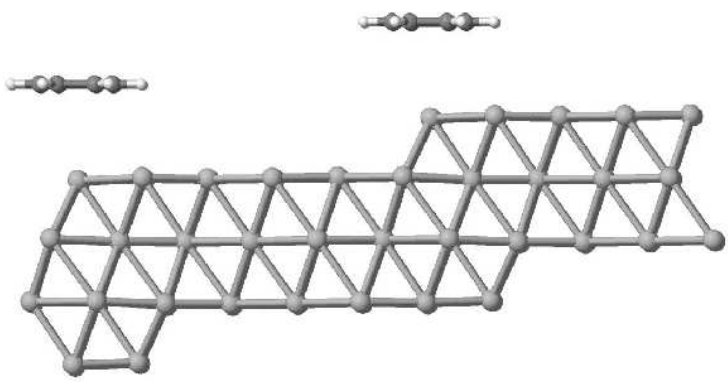

Figure 3.21: Minimum-energy configuration for the flat pentacene on Ag(233) terrace.

Table 3.10: Relative energy values, E_{rel} for flat pentacene on Ag(233) terrace. l is the distance from the low coordinated step atom and corresponding configuration on flat Ag(111) surface was given in 2nd column. E_{rel} values are relative values with respect to minimum energy configuration C.

l (Å)	configuration	E_{rel} (eV)
0.00	top-0	0.188
1.25	bridge-60	0.219
2.50	top-0	0.331
3.75	bridge-60	0.294
5.00	top-0	0.344
6.25	bridge-60	0.294
7.50	top-0	0.351
8.25	bridge-60	0.338

In addition, the flat configurations, where pentacene is placed on the terrace, were studied. The total energy increased while pentacene was moved away from the step edge (Table 3.10) and found its maximum among these flat cases where pentacene comes on top of the next step edge (Figure 3.21). In these flat cases pentacene stayed 3.70 Å above the surface, which is the same as the isolated pentacene on Ag(111). On the step edge the distance decreased to 3.65 Å. Diffusion energy barrier for the terrace seems to be low similar to the flat Ag(111)

surface. The differences in energies between adjacent bridge-60 and top-0 configurations on terrace are around 50 meV meaning a flat potential energy surface for pentacene on terrace.

With bunching all of the configurations together, energetical behaviour can be drived for the pentacene molecule on Ag(233) surface (Figure 3.22).

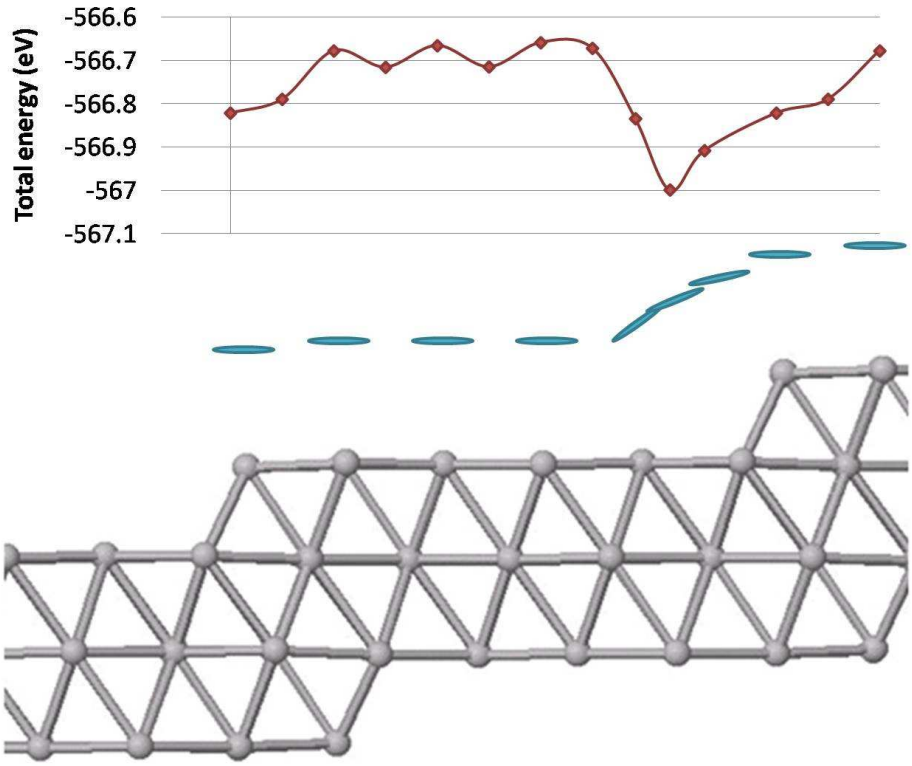

Figure 3.22: Energetical behaviour of pentacene molecule on Ag(233) surface.

The atomic positions were relaxed for the minimum energy configurations of A, B, C and for the minimum-energy flat case. The adsorption energy values are given in Table 3.11 In the flat configuration pentacene showed no distortion in terms of bond lengths and preserved planar structure. The binding energy was found to be 0.230 eV. This indicates physisorption similar to the flat Ag(111) surface. However for the configuration C, some distortions on the pentacene molecule was observed. While molecule's minimum distance with surface at terrace was ~ 3.7 Å, the distance with the low coordinated step atoms decreased to ~ 2.75 Å. Also the binding energy increased to 0.615 eV indicating stronger pentacene−surface

interactions. The bond lenghts of the terrace side of the pentacene molecule stayed the same while they increased for the step side of the molecule. Also molecule lost its planar structure and showed bending where middle of the molecule moved to the surface (Figure 3.23). Also low coordinated silver atoms below the pentacene molecule moved slightly to the molecule in agreement with the stronger interaction than the other cases.

Table 3.11: Adsorption energy values, E_{ads} for the relaxed configurations of A, B, C and flat case on Ag(233) surface.

Configuration	E_{ads} (eV)
A	−0.419
B	−0.239
C	−0.615
Flat	−0.230

More bending was observed for the step side of the pentacene molecule due to stronger interaction with step. Also the distance of ~ 2.75 Å, which is between the covalent and van der Waals seperation of the silver and carbon atoms, indicates some chemisorption character. By looking at the energetical behaviour of pentacene in Figure 3.22 one can estimate much larger diffusion barriers for the stepped case ~ 400 meV which is larger than the binding energy of 0.234 eV for the flat Ag(111) case. This indicates that step can trap the pentacene molecule on the silver surface during film growth and can act as a nucleation site, as proposed by Eremtchenko et. al. [53] and observed experimentally by Danışman et. al. [52]. Also the tilting of the molecule on the step can be related to multilayers where tilting is observed within herringbone structure in the thin films. Tilting angle on the step is found to be 17°.

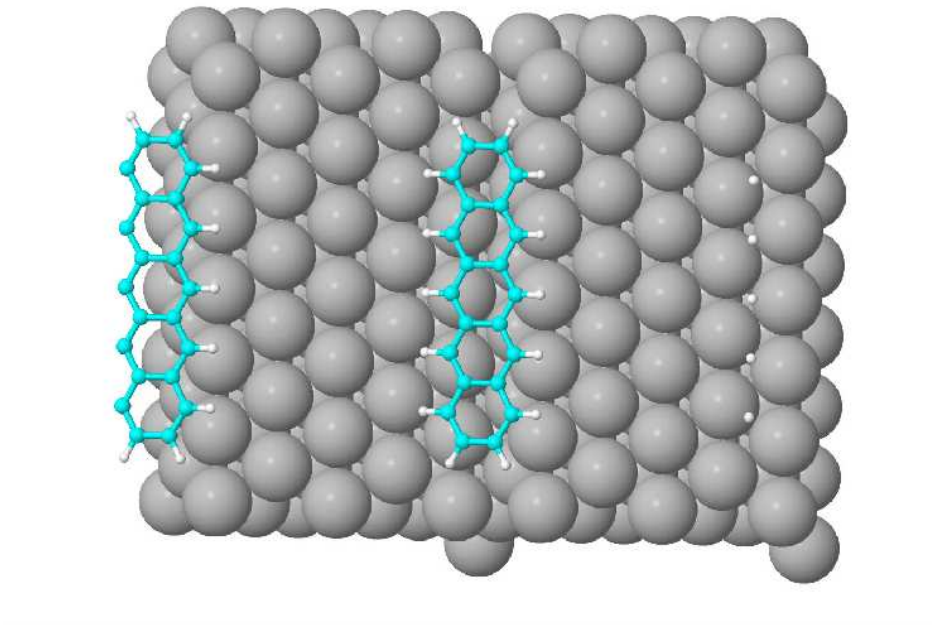

(a) top view

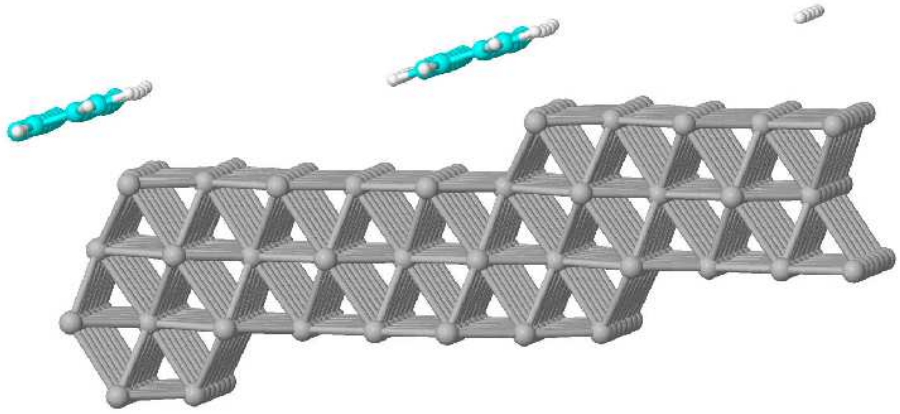

(b) side view

Figure 3.23: Relaxed geometry for configuration C.

3.5.2 Ag(799) surface

To compare the perpendicular configuration of pentacene molecule to the step, a surface with larger terrace width was needed to minimize pentacene−pentacene interactions. Therefore Ag(799) surface (Figure 3.24) was choosen where there are 9 silver atom row in the terrace. Ag(799) surface has (111) step and (111) terrace planes. 4x9 surface unit cell was choosen in this case to overcome the pentacene−pentacene interactions. The step angle is 6.5°.for this unit cell.

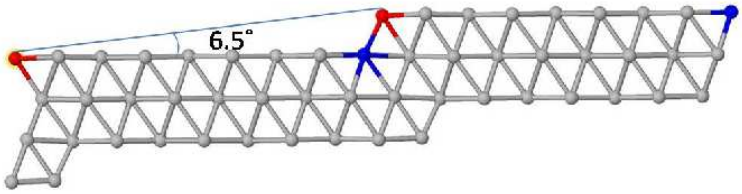

Figure 3.24: Side view of Ag(799) surface

Similar to Ag(233) surface the surface relaxations mainly occured around the step atoms. While the low coordinated silver atoms moved inwards, high coordinated silver atoms started to move outwards from the surface. Other silver atoms maintained their positions by showing very small changes in bond lengths.

In Ag(799) surface pentacene was placed perpendicular to the silver step and the energetical behaviour was studied while pentacene was moved towards the step, by performing single point calculations. Pentacene was placed on the terrace with a bridge-90 configuration since it is the lowest energy case for perpendicular arrengement with respect to the step among possible configurations. Similar to the Ag(233) surface total energy decreased while pentacene

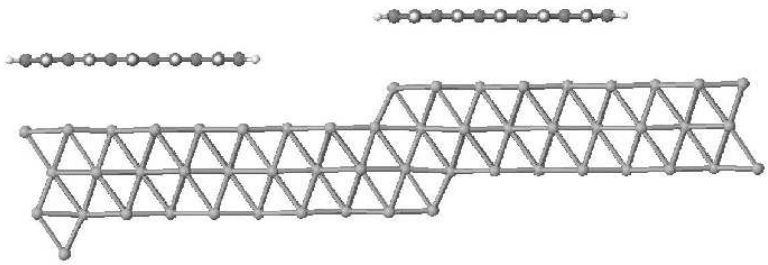

Figure 3.25: Flat pentacene on Ag(799) surface terrace with *l*=7.5 Å.

moved away from the step edge with very small energy differences showing a flat potential energy surface on the terrace (Table 3.12). The minimum energy was found where the end of the pentacene molecule came on the step edge (Figure 3.25). After this point energy started to increase because one side of pentacene molecule started to loose contact with the silver surface atoms.

Table 3.12: Relative energy values for flat pentacene on Ag(799) terrace. *l* is the distance of molecular center of pentacene from the step. E_{rel} values are relative values with respect to minimum-energy configuration *l*=7.5 Å.

l (Å)	E_{rel} (eV)
0	0.048
5	0.003
7.5	**0.000**
10	0.011
15	1.031

When pentacene was placed on the step with its long axis perpendicular to the step (Figure 3.26) the total energy did not decrease as much as the parallel case in Ag(233) surface. The minimum distance between pentacene and the step was found to be 3.2 Å. The molecule distorted so that both end of the molecule is close to the terrace. Adsorption energy was found to be 0.257 eV on the step while it was found to be 0.246 eV on the terrace of Ag(799) surface. However, adsorption energy on the step of Ag(233) where pentacene oriented parallel

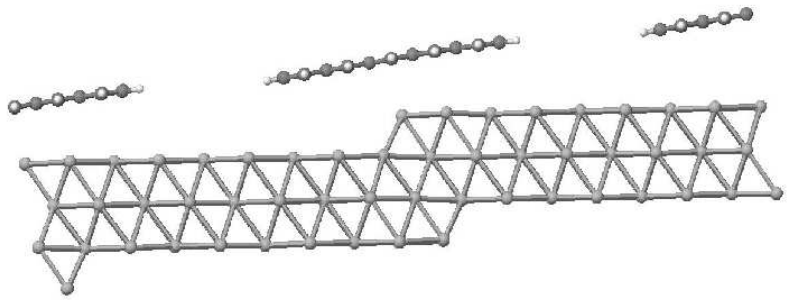

Figure 3.26: Perpendicular pentacene adsorption on Ag(799) step.

Table 3.13: Adsorption energies for pentacene on different Ag(111) surfaces.

Surface	Site	Orientation	E_{ads} (eV)
Ag(111)	terrace	flat	0.234
Ag(233)	terrace	flat	0.230
Ag(799)	terrace	flat	0.246
Ag(233)	step	parallel	0.615
Ag(799)	step	pendicular	0.257

to the step was found to be 0.615 eV (Table 3.13).

In the perpendicular orientation (Figure 3.26), interaction between step atoms and the molecule is not strong because pentacene's carbon chains could not follow the silver rows of surface and there are less carbon atoms on the molecule, which can interact with the low coordinated silver atoms. Hence, parallel configuration of pentacene is the energetically most favorable configuration in a stepped Ag(111) surface. For the flat cases on terrace the results are more or less the same as the adsorption energy on flat Ag(111) surface. This also agrees with the flat potential energy surface for pentacene on Ag(111) surface is valid on the (111) terraces. However, the flatness of the potential energy surface is distrupted by the steps on the surface. The orientation of the molecule with respect to step is determined by the potential energy surface around the step, which energetically favors parallel orientation. The step−terrace energy differences in parallel and perpendicular orientations also fit the trend where pentacene diffusion along the long molecular axis is the most favorable direction for pentacene molecule.

CHAPTER 4

CONCLUSIONS

In order to optimize device performance of a pentacene thin film transistor it is important to obtain ordered thin film structures of pentacene on the device surfaces, dielectric surface and electrode surface. On the dielectric surface, SiO_2, the literature is almost complete in terms of efficient film growth. Therefore, it is essential to optimize thin film growth on electrode surfaces via understanding the interaction between the surface and the pentacene molecule. To this end interaction between pentacene and Ag(111) surface, one of the commonly used electrode material and a model surface in surface science studies, was investigated thorougout this study and following results were obtained:

- Adsorption site for an isolated pentacene molecule on the surface was found as the bridge site with respect to molecular center of the pentacene molecule making an angle of 60° between long molecular axis of pentacene and $[0\bar{1}1]$ surface lattice direction (Figure 3.11). The adsorption energies were found as -0.155 eV and -0.234 eV with the use of GGA-PBE and GGA-PW91 exchange−correlation potentials, respectively, indicating a weak interaction between surface and pentacene as physisorption, in parallel with the corresponding adsorption height close to the sum of van der Waals radii of Ag and C atoms. No distortion on the molecule was observed, also agreeing with the proposed weak van der Waals interaction.

- Although bridge-60 configuration was found to be energetically the most favorable, all other configurations were within 40 meV of the bridge-60 configuration meaning a flat potential energy surface on Ag(111), especially along lattice directions of the surface. Hence, diffusion and rotation energy barriers were treated to be low of the order of a possible two dimensional gas phase on the surface.

- Experimentally observed thin film phases of pentacene were calculated and found energetically very close to the bulk phase of pentacene. The differences in the energy were smaller than the adsorption energies. Hence, these film polymorphs can grow on different substrates via the interaction with the surface, instead of bulk phase.

- While coverage increased to 1 monolayer, the adsorption energy decreased with the increase in adsorption height. This is mainly due to pentacene−pentacene interactions.

- Surface with steps was found to interact with pentacene stronger than the flat (111) surface case where pentacene preferred the favorable position between the low coordinated step silver atoms and the terrace atoms with a tilt angle similar to that in multilayer phases. The adsorption energy increased to 0.615 eV from 0.234 eV in the flat case. The distortions and the distances hint a chemical bonding character between pentacene and step silver atoms in addition to van der Waals interactions. This is in agreement with the proposal of thin film growth being initiated at the step edges [53, 52]. The energy profile on the stepped surface showed differences around 0.4 eV which indicates steps can trap the molecule to initiate an ordered growth.

REFERENCES

[1] Pope, M.; Swenberg, C. E.; Pope, M., Electronic processes in organic crystals and polymers, 2nd ed. **1999**.

[2] Chiang, C. K.; Fincher, C. R.; Park, Y. W.; Heeger, A. J.; Shirakawa, H.; Louis, E. J.; Gau, S. C.; Macdiarmid, A. G., *Physical Review Letters* **1977**, *39*, 1098.

[3] http://www.iapp.de/orgworld/ last visited 29/11/2009.

[4] Subramanian, V.; Frechet, J. M. J.; Chang, P. C.; Huang, D. C.; Lee, J. B.; Molesa, S. E.; Murphy, A. R.; Redinger, D. R.; Volkman, S. K. *Proceedings of the IEEE* **2005**, *93*, 1330.

[5] Gelinck, G. H.; A. Huitema, H. E.; van Veenendaal, E.; Cantatore, E.; Schrijnemakers, L.., van der Putten, J. B. P. H.; Geuns, T. C. T.; Beenhakkers, M.; Giesbers, J. B.; Huisman, B.H.; Meijer, E. J.; Benito, E. M.; Touwslager, F. J.; Marsman, A. W.; van Rens, B. J. E.; de Leeuw, D. M. *Nature Materials* **2004**, *3*, 106.

[6] Zhou, L.; Wanga, A.; Wu, S.C.; Sun, J.; Park, S.; Jackson, T. N. *Applied Physics Letters* **2006**, *88*, 083502/1.

[7] Kelley, T. W.; Baude, P. F.; Gerlach, C.; Ender, D. E.; Muyres, D.; Haase, M. A.; Vogel, D. E.; Theiss, S. D. *Chem. Mater.* **2004**, *16* (23), 4413.

[8] Kelley, T.; Boardman, L. D.; Dunbar, T. D.; Muyres, D. V.; Pellerite, M. J.; Smith, T. P. *Journal of Physical Chemistry B* **2003**, *107*, 5877.

[9] Di, C. A.; Liu, Y. Q.; Yu, G.; Zhu, D. *Accounts of Chemical Research* **2009**, *42* (10), 1573.

[10] Facchetti, A.; Yoon, M. H.; Marks, T. J. *Adv. Mater.* **2005**, *17*, 1705.

[11] de Boer, B.; Hadipour, A.; Mandoc, M. M.; van Woudenbergh, T.., Bolm, P. W. M. *Adv. Mater.* **2005**, *17*, 621.

[12] Goodings, E. P.; Mitchard, D. A.; Owen, G. *J. Chem. Soc.:Perkin Trans. 1* **1972** ,*11*, 1310.

[13] Horowitz, G. *J. Mater. Res.* **2004**, *19*, 1946.

[14] Newman, C. R.; Frisbie, C. D.; da Silva Filho, D. A.; Brodas, J.L.; Ewbank, P. C. *Chem. Mater.* **2004**, *16*, 4436.

[15] Bao, Z. *Adv. Mater.* **2000**, *12*, 227.

[16] Dimitrakopoulos, C. D.; Malenfant, P. R. L., *Adv. Mater.* **2002**, *14* (2), 99.

[17] Horowitz, G.; Fichou, D.; Peng, X.; Garnier, F. *Syntj. Met.* **1991**, *41*, 1127.

[18] Horowitz, G.; Peng, X.; Fichou, D.; Garnier, F. *Syntj. Met.* **1992**, *51*, 419.

[19] Dimitrakopoulos, C. D.; Brown, A. R.; Pomp, A. *J. Appl. Phys.* **1996**, *80*, 2501.

[20] Lin, Y.; Gundlach, D. J.; Jackson, T. N. *Ann. Dev. Res. Conf. Dig.* **1996**, 80.

[21] Lin, Y.; Gundlach, D. J.; Nelson, S.; Jackson, T. N. *IEEE Trans. Electron Devices* **1997**, *44*, 1325.

[22] Campbell, R. B.; Monteath, R. J.; Trotter, J. *Acta Crystallogr.* **1962**, *15*, 289.

[23] Mattheus, C. C.; Dros, A. B.; Baas, J.; Oostergetel, G. T.; Meetsma, A.; de Boer, J. L.; Palstra, T. T. M. *Synthetic Metals* **2003**, *138* (3), 475.

[24] Endres, R. G.; Fong, C. Y.; Yang, L. H.; Witte, G.; Woll, C. *Computational Materials Science* **2004**, *29*, 362.

[25] Parisse, P.; Ottaviano, L.; Delley, B.; Picozzi, S., *J. Phys.:Condens. Matter* **2007**, *19*, 106209.

[26] Cornil, J.; Calbert, J. P.; Bredas, J. L. *J. Am. Chem. Soc.* **2001**, *123*, 1250.

[27] Cheng, Y. C.; Silbey, R. J.; da Silva Filho, D. A.; Calbert, J. P.; Cornil, J.; Bredas, J. L. *J. Chem. Phys.* **2003**, *118*, 3764.

[28] Baude, P. F.; Ender, D. A.; Haase, M. A.; Kelley, T. W.; Muyres, D. V.; Theisse, S. D. *Appl. Phys. Lett.* **2003**, *82*, 3964.

[29] Ruiz, R.; Nickel, B.; Koch, N.; Feldman, L. C.; Haglund, R. F.; Kahn, A.; Scoles, G. *Phys. Rev. B* **2003**, *67*, 125406.

[30] Ruiz, R.; Choudhary, D.; Nickel, B.; Toccoli, T.; Chang, K. C.; Mayer, A. C.; Clancy, P.; Blakely, J. M.; Headrick, R. L.; Iannotta, S.; Malliaras, G. G. *Chem. Mater.* **2004**, *16* (23), 4497.

[31] Coropceanu, V.; Cornil, J.; da Silva, D. A.; Olivier, Y.; Silbey, R.; Bredas, J. L. *Chemical Reviews* **2007**, *107* (4), 926

[32] Fukagawa, H.; Yamane, H.; Kataoka, T.; Kera, S.; Nakamura, M.; Kudo, K.; Ueno, N. *Phys. Rev. B* **2006**, *73*, 245310.

[33] Anthony, J. E. *Angewandte Chemie–International Edition* **2008**, *47* (3), 452.

[34] Troisi, A.; Orlandi, G. *J. Phys. Chem. B* **2005**, *109* (5), 1849.

[35] Sandra, E.; Fritz, S.; Martin, M.; Frisbie, C. D.; Ward, M. D.; Toney, M. F. *J. Am. Chem. Soc.* **2004** ,*126*, 4084.

[36] Yanagisawa, H.; Tamaki, T.; Nakamura, M.; Kudo, K. *Thin Solid Films* **2004** *464-465*, 398.

[37] De Angelis, F.; Toccoli, T.; Pallaoro, A.; Coppede, N.; Mariucci, L.; Fortunato, G.; Iannotta, S. *Synthetic Metals* **2004**, *146* (3), 291.

[38] Locklin, J.; Roberts, M. E.; Mannsfeld, S. C. B.; Bao, Z. N. *Polymer Reviews* **2006**, *46* (1), 79.

[39] Pesavento, V. P.; Puntambekar, K. P.; Frisbie, C. D.; McKeen, J. C.; Ruden, P. P. *J. Appl. Phys.* **2006**, *99*, 094504.

[40] Dodabalapur, A.; Torsi, L.; Katz, H. E. *Science* **1995**, *268*, 270.

[41] Granstrom, E. L.; Frisbie, C. D. *J. Phys. Chem.* **1999**, *103*, 8842.

[42] Ihm, K; Kim, B; Kang, T; Kim, K.; Joo M.H.; Kim, T.H.; Yoon, S.S.; Chung, S. *Appl. Phys. Lett.* **2006**, *89*, 033504

[43] Lukas, S.; Sohnchen, S. ; Witte, G. ; Wöll, C. *ChemPhysChem* **2004**, *5*, 266.

[44] Kang, J. H.; Zhu, X. Y., *Appl. Phys. Lett.* **2003**, *82* (19), 3248.

[45] Kang, J. H.; Zhu, X. Y., *Chem. Mater.* **2006**, *18* (5), 1318.

[46] France, C. B.; Schroeder, P. G.; Parkinson, B. A., *Nano Letters* **2002**, *2* (7), 693.

[47] France, C. B.; Schroeder, P. G.; Forsythe, J. C.; Parkinson, B. A., *Langmuir* **2003**, *19* (4), 1274.

[48] Beernink, G.; Strunskus, T.; Witte, G.; Woll, C., *Appl. Phys. Lett.* **2004**, *85* (3), 398.

[49] Kafer, D.; Ruppel, L.; Witte, G., *Phys. Rev. B* **2007**, *75*, 085309.

[50] Kafer, D.; Witte, G., *Chem. Phys. Lett.* **2007**, *442* (4–6), 376.

[51] Casalis, L.; Danisman, M. F.; Nickel, B.; Bracco, G.; Toccoli, T.; Iannotta, S.; Scoles, G., *Phys. Rev. Lett.* **2003**, *90*, 206101.

[52] Danisman, M. F.; Casalis, L.; Scoles, G., *Phys. Rev. B* **2005**, *72*, 085404.

[53] Eremtchenko, M.; Temirov, R.; Bauer, D.; Schaefer, J. A.; Tautz, F. S., *Phys. Rev. B* **2005**, *72*, 115430.

[54] Zhang, H. L.; Chen, W.; Huang, H.; Chen, L.; Wee, A. T. S., *J. Am. Chem. Soc.* **2008**, *130* (9), 2720.

[55] Dougherty, D. B.; Jin, W.; Cullen, W. G.; Reutt-Robey, J. E.; Robey, S. W., *J. Phys. Chem. C* **2008**, *112* (51), 20334.

[56] Floreano, L.; Cossaro, A.; Cvetko, D.; Bavdek, G.; Morgante, A., *J. Phys. Chem. B* **2006**, *110* (10), 4908.

[57] Zheng, Y.; Qi, D. C.; Chandrasekhar, N.; Gao, X. Y.; Troadec, C.; Wee, A. T. S., *Langmuir* **2007**, *23* (16), 8336.

[58] Wang, Y. L.; Ji, W.; Shi, D. X.; Du, S. X.; Seidel, C.; Ma, Y. G.; Gao, H. J.; Chi, L. F.; Fuchs, H., *Phys. Rev. B* **2004**, *69*, 075408.

[59] Lee, K.; Yu, J. Y., *Surf. Sci.* **2005**, *589* (1–3), 8.

[60] Lee, K.; Yu, J. J.; Morikawa, Y., *Phys. Rev. B* **2007**, *75*, 045402.

[61] Lindstrom, C. D. ; Muntwiler, M. ; Zhu, X. Y., *J. Phys. Chem. B* **2007**, *111* (24), 6913.

[62] Ample, F.; Joachim, C., *Surf. Sci.* **2006**, *600* (16), 3243.

[63] Simeoni, M.; Picozzi, S.; Delley, B., *Surf. Sci.* **2004**, *562* (1–3), 43.

[64] Ferretti, A.; Baldacchini, C.; Calzolari, A.; Di Felice, R.; Ruini, A.; Molinari, E.; Betti, M. G., *Phys. Rev. Lett.* **2007**, *99*, 046802.

[65] Baldacchini, C.; Mariani, C.; Betti, M. G.; Vobornik, I.; Fujii, J.; Annese, E.; Rossi, G.; Ferretti, A.; Calzolari, A.; Di Felice, R.; Ruini, A.; Molinari, E., *Phys. Rev. B* **2007**, *76*, 245430.

[66] Sun, X.; Suzuki, T.; Yamauchi, Y.; Kurahashi, M.; Wang, Z. P.; Entani, S., *Surf. Sci.* **2008**, *602* (6), 1191.

[67] Satta, M.; Iacobucci, S.; Larciprete, R., *Phys. Rev. B* **2007**, *75*, 155401.

[68] Doi, K.; Yoshida, K.; Nakano, H.; Tachibana, A.; Tanabe, T.; Kojima, Y.; Okazaki, K., *J. Appl. Phys.* **2005**, *98*, 113709.

[69] Nabok, D.; Puschnig, P.; Ambrosch-Draxl, C.; Werzer, O.; Resel, R.; Smilgies, D. M., *Phys. Rev. B* **2007**, *76*, 235322.

[70] Mattheus, C. C.; de Wijs, G. A.; de Groot, R. A.; Palstra, T. T. M., *J. Am. Chem. Soc.* **2003**, *125* (20), 6323.

[71] Kresse, G.; FurthmÃ¼ller, J., *Comput. Mat. Sci.* **1996**, *6*, 15.

[72] Born, M. ; Oppenheimer, J. R. *Zur Quantentheorie der Molekeln. Ann. d. Physik* **1927**, *84*, 457.

[73] Hohenberg, P.; Kohn, W., *Physical Review* **1964**, *136* (3B), B864.

[74] Kohn, W.; Sham, L. J., *Physical Review* **1965**, *140* (4A), A1133.

[75] Kokalj, A., *Comp. Mat. Sci.* **2003**, *28*, 155.

[76] Perdew, J. P.; Chevary, J. A.; Vosko, S. H.; Jackson, K. A.; Pederson, M. R.; Singh, D. J.; and C. Fiolhais, *Phys. Rev. B* **1992**, *46*, 6671.

[77] Perdew, J. P.; Burke, K.; Ernzerhof, M. *Phys. Rev. Lett.* **1996**, *77*, 3865.

[78] Blöchl, P. E. *Phys. Rev. B* **1994**, *50*, 17953.

[79] Blöchl, P. E., *Bull. Mater. Sci.* **2003**, *26*, 33.

[80] Broyden, C. G., *Math. Comput.* **1965**, *19*, 547.

[81] Feynman, R. P., *Phys. Rev.* **1939**, *56*, 340.

[82] Moruzzi, V. L.; Janak, J. F.; Schwarz, K. *Phys. Rev. B* **1988**, *37*, 790.

[83] Hafner, J., *J. Comput. Chem.* **2008**, *29*, 2044.

[84] Li, Wei-X.; Stampfl, C.; Scheffler, M. *Phys. Rev. B* **2002**, *65*, 075407.

[85] Kadantsev, E.S.; Stott, M.J.; Rubio, A., *J. Chem. Phys.* **2006**, *124* (13), 134901.

[86] Gruhn, N. E. et al., *J. Am. Chem. Soc.* **2001**, *124*, 7918.

[87] Godby, R. W.; SchlÃ¼ter, M.; Sham, L.J., *Phys. Rev. Lett.* **1986**, *56*, 2415.

[88] Jones, R.O. ; Gunnarsson, O. ; *Rev. Mod. Phys.* **1989**, *61*, 689.

[89] Wert, C.; Zener, C., *Phys. Rev.* **1949**, *76*, 1169.

[90] Oura, K.; Lifshits, V. G.; Saranin, A. A.; Zotov, A. V., *Surface Science An Introduction* **2003**.

[91] Rousset, S. ; Reapin, V. ; Baudot, G. ; Garreau, Y. ; Lecoeur, J., *J. Phys.: Condens. Matter* **2003**, *15*, S3363.

[92] Pedio M.; Doyle B.; Mahne N.; Giglia A.; Borgatti F.; Nannarone S.; Henze S. K. M.; Temirov R.; Tautz F. S.; Casalis L.; Hudej R.; Danisman M. F.; and Nickel B., Adv. Surf. Sci. **2007**, *254* 103.